Chemical Science

ROYAL SOCIETY OF CHEMISTRY

PERSPECTIVE

View Article Online
View Journal | View Issue

Cite this: *Chem. Sci.*, 2020, **11**, 8350

All publication charges for this article have been paid for by the Royal Society of Chemistry

Received 19th June 2020
Accepted 20th July 2020

DOI: 10.1039/d0sc03429k

rsc.li/chemical-science

Heavy chalcogenide-transition metal clusters as coordination polymer nodes

Jiaze Xie, † Lei Wang † and John S. Anderson *

While metal–oxygen clusters are widely used as secondary building units in the construction of coordination polymers or metal–organic frameworks, multimetallic nodes with heavier chalcogenide atoms (S, Se, and Te) are comparatively untapped. The lower electronegativity of heavy chalcogenides means that transition metal clusters of these elements generally exhibit enhanced coupling, delocalization, and redox-flexibility. Leveraging these features in coordination polymers provides these materials with extraordinary properties in catalysis, conductivity, magnetism, and photoactivity. In this perspective, we summarize common transition metal heavy chalcogenide building blocks including polynuclear metal nodes with organothiolate/selenolate or anionic heavy chalcogenide atoms. Based on recent discoveries, we also outline potential challenges and opportunities for applications in this field.

Introduction

Coordination polymers (CPs) or metal–organic frameworks (MOFs) are an exciting class of materials due to their modular nature as well as their applicability in areas such as gas separation,[1] storage,[2] catalysis,[3] and medicine.[4] Much of the seminal work in this area has relied upon metal oxygen bonds to form nodes or secondary building units (SBUs) as exemplified by carboxylate linkers and metal oxide clusters found in MOF-5 and UiO-66.[5] While these building blocks have been enormously successful as structural units and even catalytic sites,[6] building CPs around bonds to heavier chalcogenides, such as S, Se, or Te offers many advantages. The better energetic matching between transition metals and less-electronegative heavier chalcogenides offers the possibility of enhanced coupling throughout these materials, a feature of particular importance for emerging areas such as conductive or magnetic MOFs.[7] Indeed, several new materials with remarkable properties have been made by coupling S-based ligands with monometallic nodes, an area which has received substantial recent attention.[8] The use of multi-metallic nodes with heavier chalcogenides offers similarly exciting advantages in redox activity and conductivity with potentially new directions as catalytic sites analogous to metal sulfide and selenide sites in biology and heterogeneous catalysis.[9] While this area has had several exciting recent developments, it is comparatively underexplored compared to the wealth of materials built around metal oxygen based SBUs. Here we will provide an overview of recent discoveries in this area and an outline of challenges and opportunities. We will focus on multi-metallic SBUs where anionic S, Se, or Te (as thiolate, selenolate, sulfide, selenide, or telluride) have been utilized in polynuclear transition metal nodes. We will structure the overview of these materials by focusing on specific clusters as SBUs including cases where known O-based SBUs can be modified to include heavier chalcogenides as well as new cluster morphologies featuring these elements. Closely related assemblies of polynuclear clusters in extended arrays will not be discussed, although several recent reviews are available on this topic.[10]

Structures and properties of heavy chalcogenide SBU based coordination polymers

1. Replacing oxygen with sulfur in known MOF nodes

Since Robson's seminal discovery of diamondoid Cu frameworks in the 1990's,[11] tens of thousands of MOFs have been reported as an emergent class of porous materials. The majority of these materials rely upon hard O-based linkers and SBUs which are inherently electronically insulating, limiting their utility in applications such as advanced electronics and energy storage.[12] While generating fundamentally new materials with heavy chalcogenides is an ultimate goal, a more facile strategy to endow MOFs with better charge transport properties is to replace oxygen atoms in known SBUs with less electronegative and more donating sulfur atoms. This strategy enables better predictive control over the morphology and porosity of resulting materials while enhancing electronic properties. In this section we will show some examples where selective exchange of phenolate oxygen or oxide ligands with sulfur results in improved properties.

Department of Chemistry, University of Chicago, Chicago, Illinois 60637, USA. E-mail: jsanderson@uchicago.edu

† J. X. and L. W. contributed equally.

(a) Sulfur-replacement strategies in MOF-74 (M = Mn, Fe). To realize "through-bond" charge transport, Sun *et al.* substituted the $(-M-O-)_n$ chains constituting the SBUs of MOF-74, with $(-M-S-)_n$ chains (Fig. 1B, M = Mn; Fig. 1C, M = Fe).[13a,b] By using 2,5-disulfhydrylbenzene-1,4-dicarboxylate ($DSBDC^{4-}$) instead of 2,5-dihydroxybenzene-1,4-dicarboxylate ($DOBDC^{4-}$) (Fig. 1A), two new MOF-74 analogues, $Mn_2(DSBDC)(DMF)_2$ and $Fe_2(DSBDC)(DMF)_2$ were synthesized and structurally characterized by single-crystal X-ray diffraction (SXRD, Fig. 1D). Both $Mn_2(DSBDC)$ and $Fe_2(DSBDC)$ exhibit conductivities of 2.5×10^{-12} S cm^{-1} and 3.9×10^{-6} S cm^{-1}, respectively, which are each higher by roughly one order of magnitude than their "oxygen" analogues, $Mn_2(DOBDC)$ (3.9×10^{-13} S cm^{-1}) and $Fe_2(DOBDC)$ (3.2×10^{-7} S cm^{-1}). Furthermore, analysis by flash-photolysis time-resolved microwave conductivity indicates that the charge mobility of $Mn_2(DSBDC)$ is as high as 0.02 cm^2 V^{-1} s^{-1}, comparable to that found in organic semiconductors such as polythiophenes ($\Sigma\mu$ = 0.003–0.1 cm^2 V^{-1} s^{-1})[14] and rubrene ($\Sigma\mu$ = 0.05 cm^2 V^{-1} s^{-1}), where $\Sigma\mu$ is the sum of the electron and hole mobilities.[15] These results suggest that the infinite metal–sulfur chains create a more efficient charge transport pathway. In addition to chalcogenide replacement, the authors also noted a million-fold improvement in conductivity in Fe_2(DEBDC) *versus* Mn_2(DEBDC) (E = O and S). This enhancement is assigned to lowered band gaps from additional loosely bound minority-spin carriers from the d^6 Fe(II) ions which are absent in the d^5 Mn(II) ions.[16] Later, a systematic analysis on a few Fe-based MOFs proposed that mixed valency from trace amounts of Fe(III) in these materials likely contributes to the conductivity increase as well.[17]

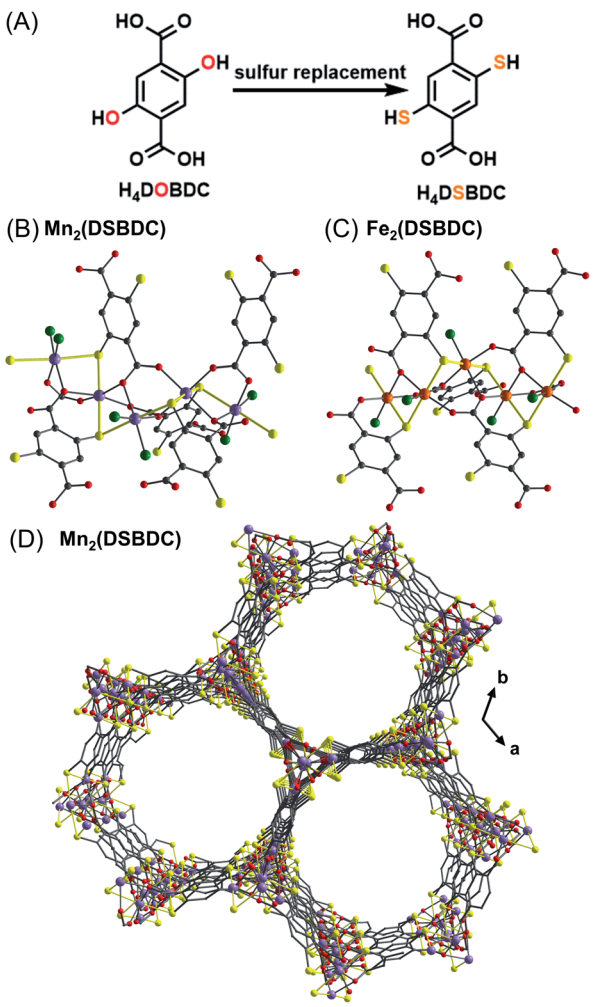

Fig. 1 Representation of a thiolate sulfur replacement strategy (A); view of an $(-M-S-)_n$ SBU in Mn_2(DSBDC) (B)[13a] and Fe_2(DSBDC) (C);[13b] view of the 1D pores in Mn_2(DSBDC), H atoms and DMF molecules have been omitted for clarity (D). Color code: S, yellow; O, red; C, grey; Mn, purple; Fe, orange; DMF O, green.

Recently, Sun *et al.* also investigated the effects of DMF guest molecules on the electrical conductivity of Fe_2(DSBDC).[13c] Three phases were isolated—a solvated phase, $Fe_2(DSBDC)(DMF)_2 \cdot x(DMF)$; a DMF-coordinated phase, $Fe_2(DSBDC)(DMF)_2$; and an activated phase, Fe_2(DSBDC). It was found that stepwise removal of unbound and coordinated DMF causes the conductivity to decrease by 1 or 2 orders of magnitude, respectively. Density functional theory (DFT) calculations suggest that DMF binding does not affect charge mobility but instead increases the concentration of holes as charge carriers.

These systems can be considered dimensionally reduced versions of all inorganic metal–chalcogenides and demonstrate that enhanced redox-matching from metal–sulfur bonding provides better charge transport pathways.[18]

(b) Substituting sulfide for oxide. While thiolates can be synthesized and used as components in solvothermal synthesis, sulfide can be more difficult to incorporate synthetically. Nevertheless, inclusion of dianionic sulfide should result in even greater covalency and orbital overlap than thiolates, and there have been some efforts that have shown that sulfide congeners of known oxide-based nodes can be generated (Fig. 2A).

The SBU containing square-planar tetra-coordinated oxygen (sptO) was first discovered in PCN-9 by the Zhou group in 2006.[19] In the same year, Dincă *et al.* reported a related square-planar Mn_4Cl building block.[20] Although more cases of sptO/Cl were reported later,[21] the square-planar tetra-coordinated sulfur (sptS) SBU has been harder to generate and has only recently been observed in the new material MCOF-89 by Yang *et al.*[22] MCOF-89 was synthesized through a high-temperature (190 °C) solvothermal reaction of 1,3,5-benzenetricarboxylic acid, $Mn(O_2CMe)_2$ and thiourea in a mixed solvent of DMF and 1,8-diazabicyclo[5.4.0]undec-7-ene (DBU). The topology of MCOF-89 (Fig. 2D) belongs to the (3,8)-connected network family with two kinds of cages, a truncated octahedral cage and a cuboctahedral cage, as is observed in other MOFs based on M_4Cl or M_4O SBUs. The former cage is constructed by six $[Mn_4(\mu_4\text{-}S)]$ squares (Fig. 2B and C) and the latter is composed of 12 SBUs. Although the metal chalcogenide units are separated in the framework, the optical bandgap of MCOF-89 is 2.82 eV, which is in the range of semiconducting materials and significantly smaller than other Mn-BTC MOFs.[23] In addition, indium tin oxide (ITO) photoelectrodes with deposited MCOF-89 generate a photocurrent density of ~1.9 μA cm^{-2}, which is also larger than that of MOF–Mn-BTC-1 (ref. 23*b*) and further

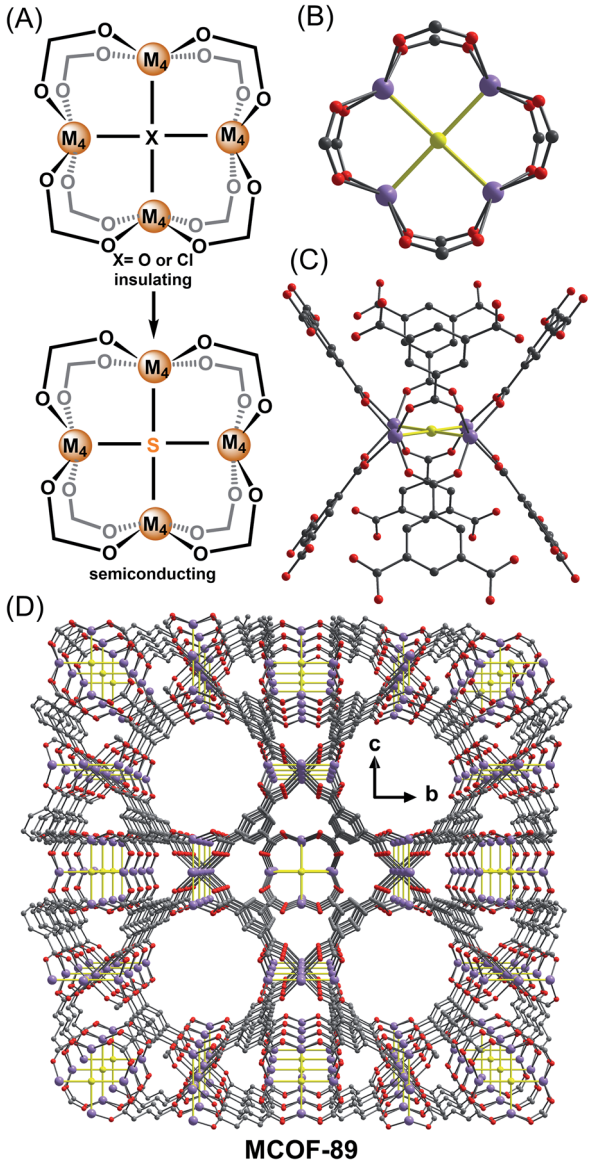

Fig. 2 Representation of a sulfide substitution strategy (A); ball-and-stick depictions of the coordination environment of the Mn_4S SBU (B) and (C); the three-dimensional open framework of MCOF-89 (D).[22] Color code: S, yellow; O, red; C, grey; Mn, purple.

supports semiconducting character in MCOF-89. While the delocalization of this system may still be limited by the use of carboxylate linkers, the changes in bandgap and photocurrent likely arise from enhanced coupling within the SBUs due to the substitution for sulfur.

2. Self-assembled transition metal–thiolate/selenolate cluster SBUs

Polynuclear transition metal complexes supported by soft donor (*i.e.* S, Se, Te) containing ligands have been increasingly receiving attention not only because of their intrinsic structural diversity but also their potential application in non-linear optics (NLO), magnetism, electrochemistry, and catalysis.[8,24] Investigations have demonstrated that molecular properties such as magnetic exchange can be enhanced using soft donor containing ligands as compared to harder donors like oxygen.[25] Nevertheless, significant challenges for the rational design and synthesis of these complexes remain, such as controlling their size and nuclearity. Novel or unexpected products can also form due to the flexible coordination geometry of metal–chalcogenolate bonds.[26] The generation of CPs with metal–chalcogenolate based SBUs without oxygen analogues faces challenges that parallel those found in molecular systems, and examples of well-defined CPs featuring these building blocks are rare. Only a few examples have been reported so far using organosulfur or organoselenide ligands for the *in situ* generation of discrete metal–thiolate clusters or infinite metal–thiolate/selenolate SBUs, but these materials display promising magnetic interactions and electrical conductivity.

(a) Discrete metal–thiolate clusters as SBUs. Multi-metallic metal–oxygen clusters based on carboxylate ligands are widely used as SBUs in the construction of MOFs.[27] These clusters are typically rigid with discrete shapes which make them useful in predicting the topology of resulting MOFs based on the geometry of the SBU. For instance, in the crystal structure of MOF-31, the four carboxylate C atoms in each $Zn(CO_2)_4$ cluster can be viewed as a tetrahedral inorganic SBU which can extend into a diamond network when linked by linear spacers such as acetylenyl (C≡C).[26a] In contrast to common oxygen-based SBUs, metal–thiolate clusters have been used as SBUs far less frequently, and thus predicting the morphology of materials with these SBUs can be more complicated. One early example of a metal–thiolate polymer, $[Ni_2(C_4H_3N_2S)_4]_n$, was isolated through a hydrothermal reaction of $Ni(O_2CMe)_2$ with pyrimidine-2-thiol by Zhao *et al.*[28] The polymer has a lamellar structure and the smallest repeating unit is a $Ni_2(C_4H_3N_2S)_4$ dimeric cluster (Fig. 3A and B). Magnetometry shows that $\chi_M T = 2.60\ cm^3\ K^{-1}\ mol^{-1}$ per dimer at 299 K but increases slightly upon cooling to a maximum value of $2.78\ cm^3\ K^{-1}\ mol^{-1}$ at 60 K before abruptly decreasing to $1.44\ cm^3\ K^{-1}\ mol^{-1}$ at 7.9 K. Fitting this magnetic data suggests the existence of ferromagnetic interactions between the two Ni centers in the $[Ni_2S_4]$ clusters with antiferromagnetic interactions between both adjacent clusters and adjacent layers. Solid state $[Ni_2(C_4H_3N_2S)_4]_n$ also exhibits a conductivity of 5×10^{-3} S cm^{-1} at 28 °C.

Similarly, employing the heterocyclic 2-mercaptonicotinic acid (mna) as a ligand under hydrothermal conditions enables the preparation of a new 2D framework formulated as $[Ni_9(mna)_{10}(H_2O)_{10}]\cdot(H_2O)_{13}$.[29] This 2D (4,4)-topological network features heptanuclear $[Ni_7S_{10}]$ clusters which are some of the largest discrete nickel–sulfur SBUs in any 2D coordination network (Fig. 3C). These clusters are linked by binuclear nickel oxygen $[Ni_2O_2]$ nodes to generate the 2D framework (Fig. 3D). Interestingly, the sulfur atoms adopt two different μ_2- and μ_3-binding modes and the authors propose that the latter are crucial for the stabilization of the cluster. The experimental $\chi_M T$ value per $[Ni_9]$ unit is $6.38\ cm^3\ K^{-1}\ mol^{-1}$ at room temperature, which is considerably lower than the expected theoretical value for nine non-interacting $S = 1$ Ni centers ($9\ cm^3\ K^{-1}\ mol^{-1}$) and likely suggests antiferromagnetic exchange coupling in the $[Ni_9]$ units.

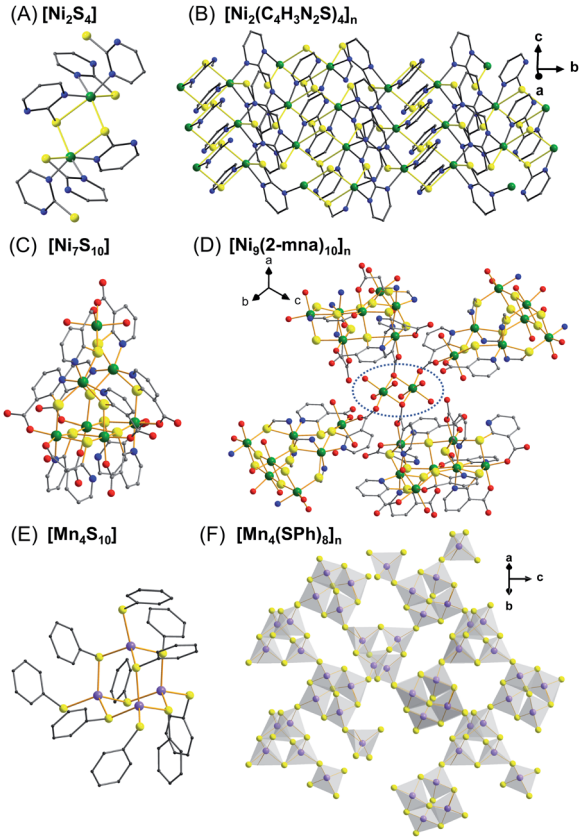

Fig. 3 Discrete metal thiolate clusters as SBUs. Representation of the $[Ni_2S_4]$ cluster (A) and the lamellar metal–thiolate polymer $[Ni_2(C_4H_3N_2S)_4]_n$ (B);[28] the heptanuclear $[Ni_7S_{10}]$ cluster (C) and its corresponding connection in the 2D framework of $[Ni_9(2\text{-mna})_{10}]_n$ (D);[29] the $[Mn_4S_{10}]$ clusters (E) and the adamantoid 3D network formed by the cluster units in $[Mn_4(SPh)_8]_n$ (F).[30] Color code: S, yellow; O, red; C, grey; N, blue; Mn, purple; Ni, green.

Outside of group 10, there is also an interesting 3D framework containing $[Mn_4(SPh)_{10}]$ clusters that has been reported by Eichhöfer *et al.*[30] Four Mn atoms and six μ_2-bridging SPh ligands constitute adamantanoid cages (Fig. 3E) and extend in three dimensions through four additional μ_2-bridging benzenethiolate ligands (Fig. 3F). The magnetic behavior of this material was studied between 2 K and 300 K with a field of 100 Oe. The continual decrease of $\chi_M T$ with decreasing temperature indicates the presence of antiferromagnetic interactions. Fitting the $\chi_M T$ *vs.* T data provides an antiferromagnetic coupling constant of $J = -8.2$ cm^{-1} assuming six equal exchange pathways between the Mn(II) ions through the SPh- bridges for an isolated Mn_4 cluster. This material also emits brightly in the red/near infrared below 100 K with a relatively large Stokes shift. This red emission, in contrast to a characteristic green-to-orange emission for Mn(II) d–d transitions, is ascribed to triplet excitations arising from the Mn(II), S(Se) bridges, and phenyl(mesityl) ligands. This observation may suggest some degree of delocalization throughout this network, but experimental evidence for this hypothesis has not yet been reported.

(b) Coordination polymers with infinite (–M–S/Se–)$_n$ SBUs. The bridging ability of thiolate/selenolate ligands frequently leads to the formation of infinite SBUs as opposed to discrete clusters with transition metals. For instance, a series of 1D CPs with the formula $[M(SR)_2]_n$ (M = Fe, Co; R = Ph, Mes, Mes = 2,4,6-$Me_3C_6H_2$) and $[M(SeR)_2]_n$ (M = Fe, Mn; R = Ph, Mes) have been reported.[31] The formation of polymeric structures rather than monomeric, dimeric, or oligomeric structures depends on the steric demand of the organic ligands, with smaller linkers favoring polymers. These polymeric chains generally display antiferromagnetic coupling and, analogous to classic studies on coupling in oxide materials,[32] magnetic measurements reveal that the bridging angle can strongly influence the antiferromagnetic exchange interactions along the chain. An illustration of this comes from comparing the structures and properties of $[Fe(SR)_2]_n$ chains.[31d] The four-membered Fe_2S_2 rings in $[Fe(SPh)_2]_n$ (Fig. 4A) display a butterfly shape (75.22° for the Fe–S–Fe bridging angle) while the rings are more planar and closer to a square in $[Fe(SMes)_2]_n$ (91.38°, Fig. 4B). The more acute bridging angle in the former chain gives rise to a stronger antiferromagnetic exchange interaction based on magnetic analysis.

In addition to 1D polymers, 2D and 3D networks with infinite $(–M–S/Se–)_n$ chains have been reported using either mixed thiolate–pyridyl or thiolate–carboxylate ligands. These materials also display unique magnetic properties.

The reaction of $CoCl_2 \cdot 6H_2O$ with the thiosalicylate dianion under hydrothermal conditions yields a new crystalline polynuclear phase, $[Co((O_2C)(S)C_6H_4)]_n$, rather than the molecular complexes formed under ambient conditions.[33a] The overall topology is a complicated 2D layered network where the neighboring Co(II) centers are bridged in three modes, Co–S–Co, Co–O–Co, and Co–OCO–Co. The infinite Co–S–Co chains form parallel to the crystallographic c axis (Fig. 4C).

Magnetic measurements show a steady decrease in moment with temperature for $[Co((O_2C)(S)C_6H_4)]_n$ before a sharp increase at 9 K which is suggestive of long-range magnetic interactions. Fitting to the Curie–Weiss law in the high temperature region (above 100 K) provides a large negative value for the Weiss constant of $\theta = -585(3)$ K, indicating strong antiferromagnetic coupling. The greater covalency of Co–S bonding than Co–O bonding makes it likely that the Co–S lattice is responsible for the magnitude of these antiferromagnetic interactions. The strength of the applied field was varied to explain the peak at low temperature. The observation that weaker applied fields induce higher magnetization suggests that antiferromagnetic coupling with spin canting is the origin of this feature.

It is worth noting that recently this polymer was also grown as nanosheet arrays on Ni foil. This composite has been explored as a battery-type electrode for an asymmetric supercapacitor.[33b] While powders of $[Co((O_2C)(S)C_6H_4)]_n$ show poor electrochemical performance, nanosheets deposited on Ni foils display pseudocapacitive behaviors with high specific capacitance of 759 F g^{-1}, good rate performance (58.8% at 10 A g^{-1}), and excellent cycling stability (73.4% retention after 5000 cycles). The faradaic process was assigned to a Co(II)/Co(III) redox couple and this proposal is supported by X-ray photoelectron spectroscopy (XPS).

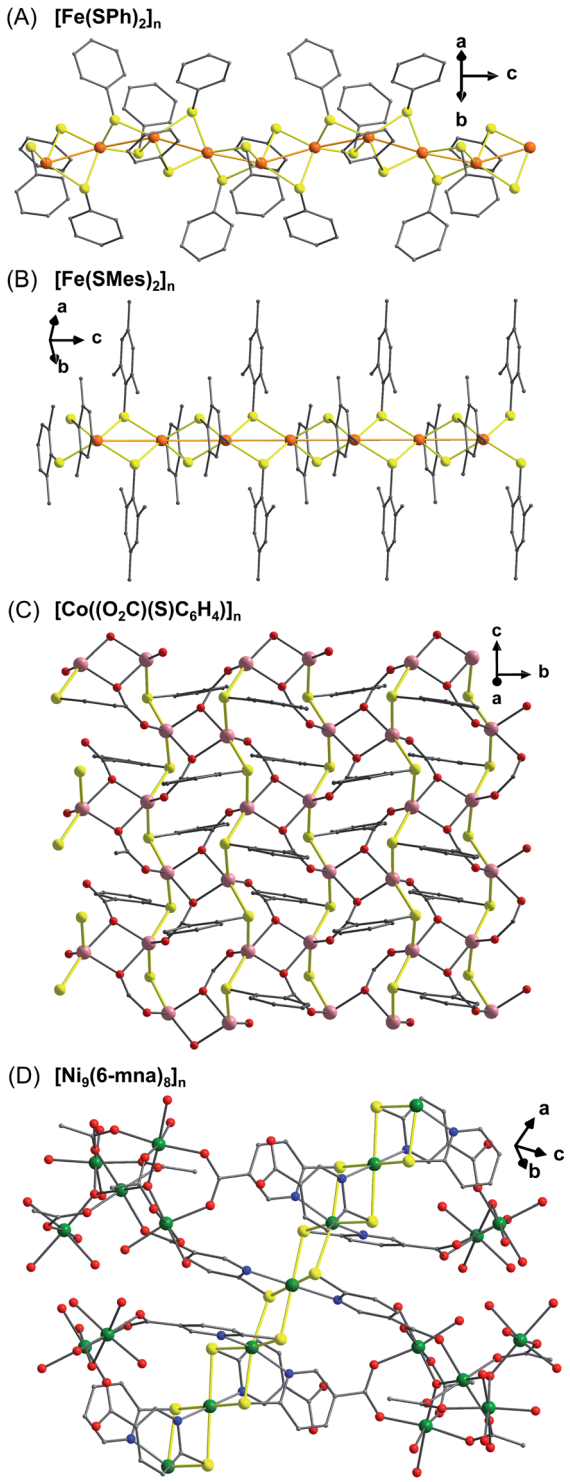

Fig. 4 Infinite $(-M-S-)_n$ chains in representative 1D polymers $[Fe(SPh)_2]_n$ (A), $[Fe(SMes)_2]_n$ (B),[31d] the 2D polymer $[Co((O_2C)(S)C_6H_4)]_n$ (C)[33a] and the 3D polymer $[Ni_9(6\text{-mna})_8]_n$ (D).[34] Color code: S, yellow; O, red; C, grey; N, blue; Fe, orange; Co, rose; Ni, green.

Similarly, using 6-mercaptonicotinic acid (6-mna) with Co(II) or Ni(II) leads to 3D frameworks with antiferromagnetic interactions containing both isolated metal–thiolate clusters and infinite M–S chains.[34] However, only the Ni complex has been characterized by SXRD. As shown in Fig. 4D, there are two distinct coordination environments for the Ni centers. One shows octahedral Ni(II) ions chelated by two 6-mna ligands *via* four equatorial thiolate sulfurs in a square plane and two pyridine nitrogens arranged *trans* at the apical sites. These Ni octahedra are edge-sharing and thus form an undulating chain of $Ni-S_4$ squares. The other Ni species exist as isolated Ni_5 clusters which are bridged by *syn*,*syn*-OCO-carboxylate and *cis*-solvent molecules. These clusters connect the infinite Ni–S chains into a 3D network. While the Weiss constant of −17.5 K indicates antiferromagnetic coupling as the dominant exchange interaction, the $\chi_M T$ of these Ni polymers shows a peak at 14 K which decreases with increasing magnetic field suggesting the presence of spin-canting.

The materials described above leverage M–S linkages for interesting magnetic behaviors, but this design element also enables high electrical conductivity. Two 2D π–d conjugated CPs with planar 2D Kagomè lattices and a formula of $[Cu_3(C_6Q_6)]_n$ (Q = S, Se) have been prepared from Cu(II) and benzenehexathiolate (BHT)/benzenehexaselenolate (BHSe) by the Zhu group.[35] In these two structures each ligand is connected to six Cu(II) ions to generate six-fold symmetry. Each Cu atom is coordinated to four μ_2–S in a square-planar geometry leading to a dense nonporous network with infinite (–Cu–S/Se–) linkages (Fig. 5A). The conductivity of a pressed pellet of $[Cu_3(C_6Se_6)]_n$ is 110 S cm^{-1} and a thin film of $[Cu_3(C_6S_6)]_n$

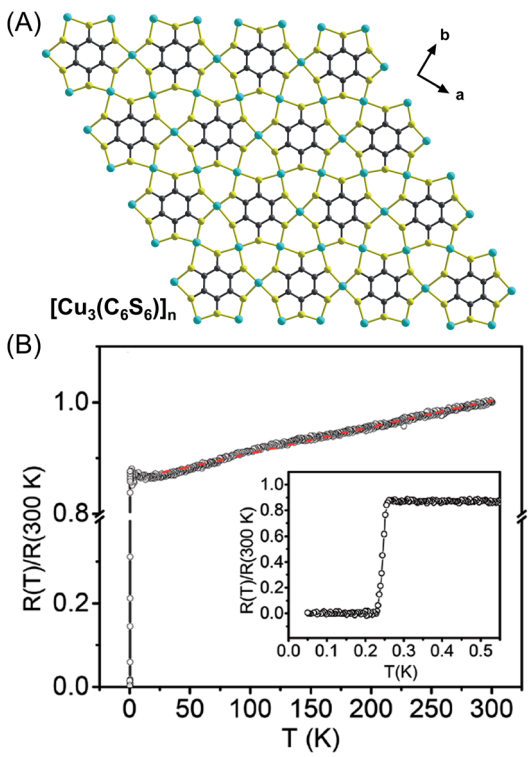

Fig. 5 The planar 2D Kagomè lattice of $[Cu_3(C_6S_6)]_n$ (A). Color code: S, yellow; C, grey; Cu, sky blue.[35b] Temperature dependence of the normalized resistance $R(T)/R$ (300 K). Inset: expanded scale for temperatures near the superconducting transition (B) (reproduced from ref. 35*b* with permission from Wiley-VCH, copyright 2017).

displays a conductivity of 2500 S cm^{-1} at room temperature, which is the highest among reported CPs. Ultraviolet photoelectron spectroscopy (UPS) on both materials suggests a Fermi edge above 0 consistent with an intrinsic metallic nature in these materials and provides an explanation for the observed high conductivity. Furthermore, a superconducting transition was observed at $T_c = 0.25$ K at ambient pressure for $[Cu_3(C_6S_6)]_n$ as indicated by electrical resistivity, magnetic susceptibility, and specific heat measurements, making it the first and only example of a CP that exhibits superconductivity (Fig. 5B). Meanwhile, under field-effect modulation, $[Cu_3(C_6S_6)]_n$ displays ambipolar charge transport with extremely high electron and hole mobilities (116 $cm^2 V^{-1} s^{-1}$ for electrons and 99 $cm^2 V^{-1} s^{-1}$ for holes). In short, the unique Kagomè topologies of these materials and extraordinary conductivity highlight the great potential in designing new superconducting and advanced electronic materials from transition metal-heavy chalcogenide SBUs.

3. Discrete transition metal sulfide/selenide/telluride clusters as nodes

While the strategy of using organosulfur or organoselenide ligands to generate metal–thiolate/selenolate SBUs directly in the construction of CPs has been remarkably successful, preformed transition metal sulfide/selenide/telluride clusters are also attractive SBUs for new materials. Transition metal–chalcogenide clusters, here defined as polynuclear complexes with multiple metal–chalcogenide (S, Se, Te) bonds, have been investigated for some time as mimics or molecular analogues of chalcogenide minerals.[36] These clusters are potentially useful building blocks in the construction of functional materials because of their tunable structural diversity, catalytic activity, multiple accessible redox states, and magnetic properties. Several examples have been reported so far using known metal sulfide/selenide/telluride clusters as nodes either through ligand substitution or "complex as ligand" methodologies,[37] but the utility of these building blocks is vastly underexplored relative to oxygen-based alternatives.

(a) Coordination polymers based on Mo_3S_7 clusters. Molybdenum disulfide (MoS_2), especially as nanoparticles or monolayers, is an active catalyst for the hydrogen evolution reaction (HER) and thus is a popular research target in the field of renewable energy.[38] Since the fundamental mechanism of catalysis is still under debate, molecular clusters such as $Mo_3S_7^{4+}$ have been targeted as models of MoS_2 as these species demonstrate an ideal topology to mimic the active sites in mechanistic studies.[39]

Recently, Ji *et al.* have successfully linked Mo_3S_7 clusters with 1,4-benzenedithiolate (BDT) to form dimers, cages, and 1D chains.[40] The robust ligand substitution chemistry of the well-documented Mo_3S_7 clusters enables its extension into chains as a three-connected SBU (Fig. 6A). The highly crystalline chains of MOS-3 (Fig. 6B) display dramatically improved catalytic activity for HER with a 40-fold enhancement in turnover frequency (TOF) over molecular Mo_3S_7-cluster complexes. This material also enables electrocatalysis with a current density of

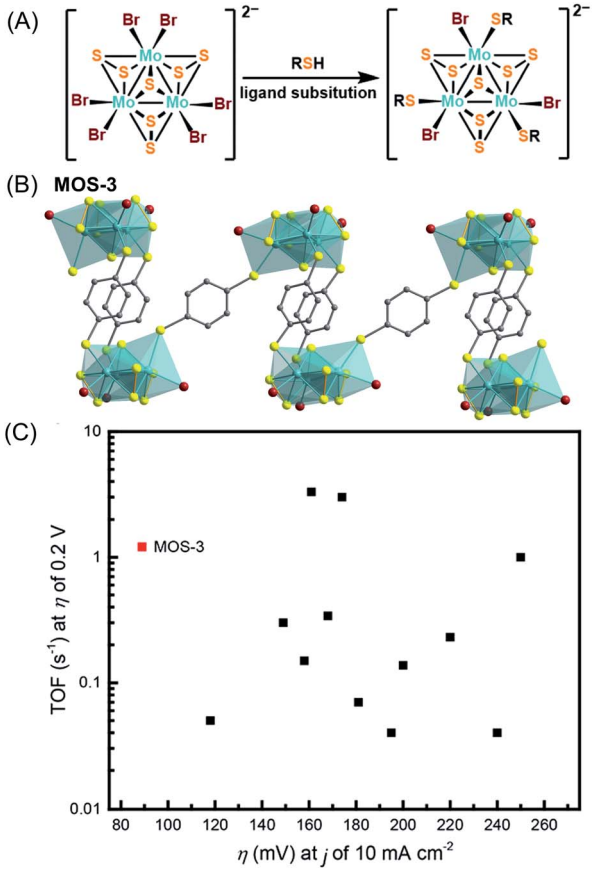

Fig. 6 Representation of a ligand substitution strategy (A);[40] Mo_3S_7 clusters connected by BDT into a chain structure (MOS-3) (B). Color code: Br, orange; S, yellow; C, grey; Mo, light green. Comparison of HER catalysts between MOS-3 (red dot) and various inorganic MoS_x materials (black dots): TOF per Mo at an overpotential (η) of 0.2 V plotted against the overpotential required for a current density of 10 mA cm^{-2} (C) (reproduced from ref. 40 with permission from the American Chemical Society, copyright 2018).

10 mA cm^{-2} at an overpotential of only 89 mV, representing the lowest value among both molecular and solid-state Mo–S_x compounds (Fig. 6C). This outstanding performance is ascribed to the periodic arrangement of Mo_3S_7 clusters on the electrodes facilitating mass transport. Unlike previous catalytic studies on amorphous MoS_2 materials, highly crystalline polymers allow for analysis on well-defined structures at the molecular level. This advance also enables straightforward synthesis and processing onto electrodes or devices.

(b) Coordination polymers based on Fe_4S_4 clusters. Iron–sulfur clusters were first discovered in ferredoxins in the early 1960s, and more than 120 distinct types of enzymes and proteins containing these clusters have been identified since then.[9a,41] These enzymes are generally involved in redox processes which are enabled by the various oxidation states of the iron–sulfur clusters. A variety of synthetic molecular clusters have been investigated as mimics of these important cofactors. In the family of iron–sulfur clusters nuclearities can range from 2 to 18 with as many as 30 bridging sulfur (sulfide) atoms, resulting in diverse geometric and electronic structures.[42] The diverse structures and

redox properties of this family of clusters make them ideal candidates as SBUs. However, incorporating these iron–sulfur clusters into CPs has only recently been explored.

Recently, Horwitz, Xie, *et al.* demonstrated that the most thoroughly studied Fe_4S_4 clusters can be connected with BDT through solvothermal reactions between $BDTH_2$ and $[NR_4]_2[Fe_4S_4](SPh)_4$ (R = methyl or *n*-butyl groups) to generate highly crystalline 1D-chain polymers (Fig. 7A).[43] The crystallinity of these chains is possibly due to slow or reversible ligand substitution processes between BDT and benzenethiolate. Furthermore, it was found that anionic chains exhibited counterion dependent solubility. The tetramethylammonium (TMA) salt is soluble in DMF and small-angle X-ray scattering (SAXS) confirms that the anionic chains exist as swollen polymer coils in solution. Taking advantage of this solubility, the electronic properties of Fe_4S_4–BDT chains were probed *via* UV-visible spectroscopy and cyclic voltammetry and compared to the $\{[Fe_4S_4](SPh)_4\}^{2-}$ precursors. Importantly, two quasi-reversible reduction processes are observed for the chain material which are assigned as the $[Fe_4S_4]^{2+}/[Fe_4S_4]^{+}$ and $[Fe_4S_4]^{+}/[Fe_4S_4]^{0}$ couples respectively (Fig. 7B). Further studies show that the redox-activity of the Fe_4S_4 clusters can be accessed with chemical reagents as post-synthetic reduction increases the electrical conductivity of the materials by up to 4 orders of magnitude from $5(3) \times 10^{-10}$ to $5(2) \times 10^{-6}$ S cm^{-1}.

These results highlight the advantages of using redox-active metal–chalcogenide clusters as building blocks in preparing new classes of CPs with tuneable properties, but it is noteworthy that there are comparatively few examples where well-defined sulfide clusters have been used in this manner.

(c) Coordination polymers based on $[TeFe_3(CO)_9Cu_2]$ clusters. Transition metal carbonyl complexes have been known for more than 100 years and are classic case studies in organometallic chemistry. Many metal carbonyl clusters exhibit redox-activity and can serve as electron reservoirs. Thus, they may serve as functional nodes for CPs.[44] Among the family of transition metal carbonyl clusters, carbonyl chalcogenide clusters have emerged as a unique subclass and this area has matured over the past few decades.[45] Incorporation of these clusters into extended structures through organic linkers has

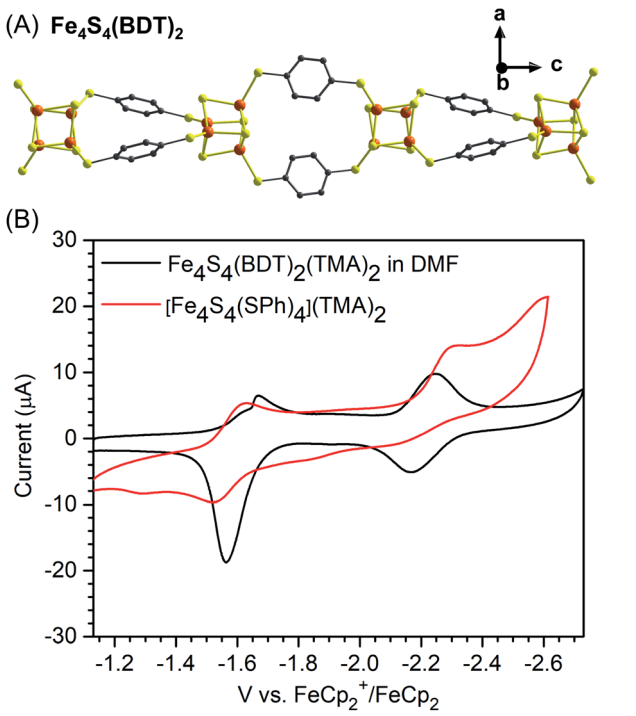

Fig. 7 Structural representation of $[Fe_4S_4(BDT)_2]^{2-}$ anion chains (A). Color code: S, yellow; C, grey; Fe, orange.[43] Cyclic voltammograms of polymer $Fe_4S_4(BDT)_2(TMA)_2$ and monomeric $[Fe_4S_4(SPh)_4][TMA]_2$. Conditions: DMF, 0.1 M $[Li][CF_3SO_3]$, 0.1 V s^{-1} (B) (reproduced from ref. 43 with permission from the American Chemical Society, copyright 2019).

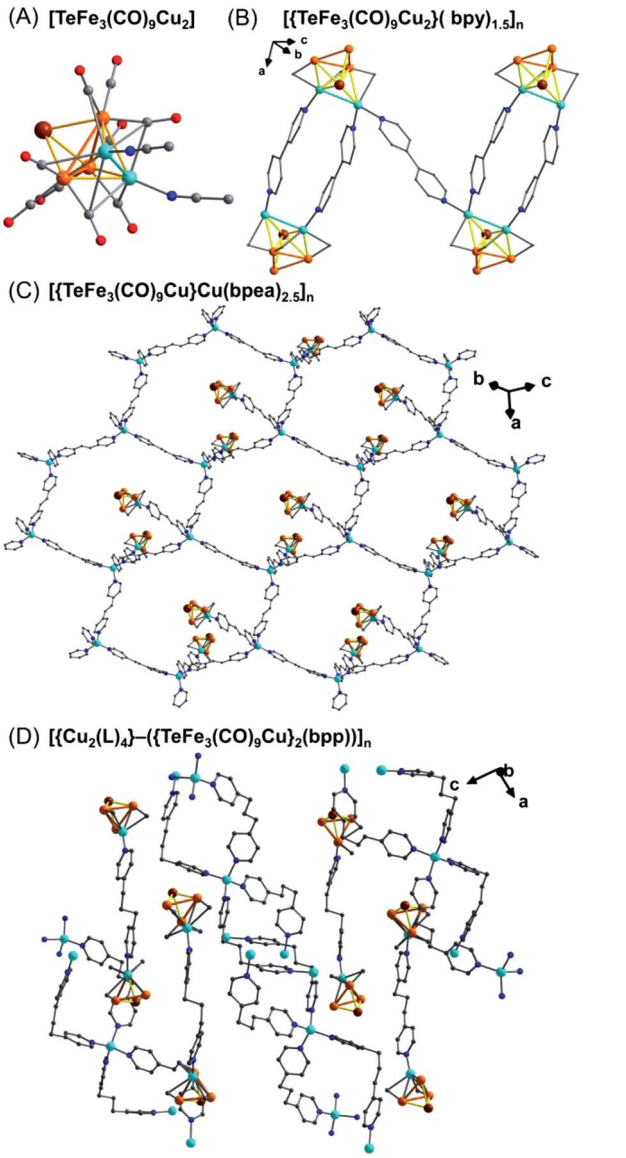

Fig. 8 Schematic representation of the $TeFe_3(CO)_9Cu_2(MeCN)_2$ cluster (A); a 1D zigzag chain of $[\{TeFe_3(CO)_9Cu_2\}(bpy)_{1.5}]_n$ (B);[46a] 2D honeycomb-like polymers of $[\{TeFe_3(CO)_9Cu\}Cu(L)_{2.5}]_n$ (L = bpea) (C); a 2D wave-like cation–anion polymer of $[\{Cu_2(L)_4\}–(\{TeFe_3(CO)_9Cu\}_2(L))]_n$ (L = bpp) (D).[46b] Color code: Te, brown; O, red; N, blue; C, grey; Fe, orange; Cu, sky blue. CO has been omitted for clarity.

been explored in only a limited manner, with a few examples of CPs reported so far using dipyridyl ligands and the $[TeFe_3(CO)_9Cu_2]$ cluster.[46]

A particularly important example is the ternary Te–Fe–Cu polymer chain $[\{TeFe_3(CO)_9Cu_2\}(bpy)_{1.5}]_n$ (bpy = μ-4,4′-dipyridyl) which is prepared from the parent cluster $[Et_4N]_2[TeFe_3(CO)_9]$, $[Cu(MeCN)_4][BF_4]$ and bpy in a one-pot reaction.[46a] Alternatively, crystalline polymer chains can also be obtained by generating the neutral cluster $TeFe_3(CO)_9Cu_2(MeCN)_2$ (Fig. 8A) first and then reacting with organic linkers. SXRD analysis shows that the polymer chain consists of the $[TeFe_3(CO)_9Cu_2]$ units alternately linked by single and pairs of bpy ligands in a zigzag fashion (Fig. 8B). Furthermore, this material exhibits semiconducting behavior with low band gaps of ~0.41 eV. This behavior is ascribed to the extended structure and the π–π interactions between the paired bpy ligands based on DFT calculations. Later, a series of CPs were prepared *via* mechanochemical synthesis using $TeFe_3(CO)_9Cu_2(MeCN)_2$ as a precursor with different dipyridyl linkers, including a 1D zigzag polymer $[\{TeFe_3(CO)_9Cu_2\}(L)]_n$ (L = 1,2-bis(4-pyridyl) ethane (bpea) or 1,2-bis(4-pyridyl)ethylene (bpee)), 2D honeycomb like polymers $[\{TeFe_3(CO)_9Cu\}Cu(L)_{2.5}]_n$ (L = bpea or bpee) (Fig. 8C), and 2D wave-like charged polymers $[\{Cu_2(L)_4\}–(\{TeFe_3(CO)_9Cu\}_2(L))]_n$ (L = 1,3-bis(4-pyridyl)propane (bpp)) (Fig. 8D).[46b] All of these materials are semiconducting. Surprisingly, the $[\{Cu_2(L)_4\}–(\{TeFe_3(CO)_9Cu\}_2(bpp))]_n$ material, which uses the bpp ligand that has no extended conjugation, exhibits better semiconducting characteristics with a bandgap of 1.43 eV and a conductivity of 1.5×10^{-2} S cm^{-1}.

(d) Coordination polymers based on M_6Q_8 clusters. Over the past few decades, a family of octahedral molecular transition metal–chalcogenide clusters with the general formula M_6Q_8 (M = V, Cr, Co, Fe, Mo, W; Q = S, Se) have been actively studied. These molecules represent the minimum units in solid Chevrel phases used for superconductivity, fast ion conductivity, thermoelectrics, and catalysis.[47] These clusters consist of a regular M_6 octahedron face-capped by eight chalcogenide atoms Q and are accessible through solution chemistry.[36a,48] The physical properties of these molecular precursors make them attractive building blocks for CPs, and there have been several

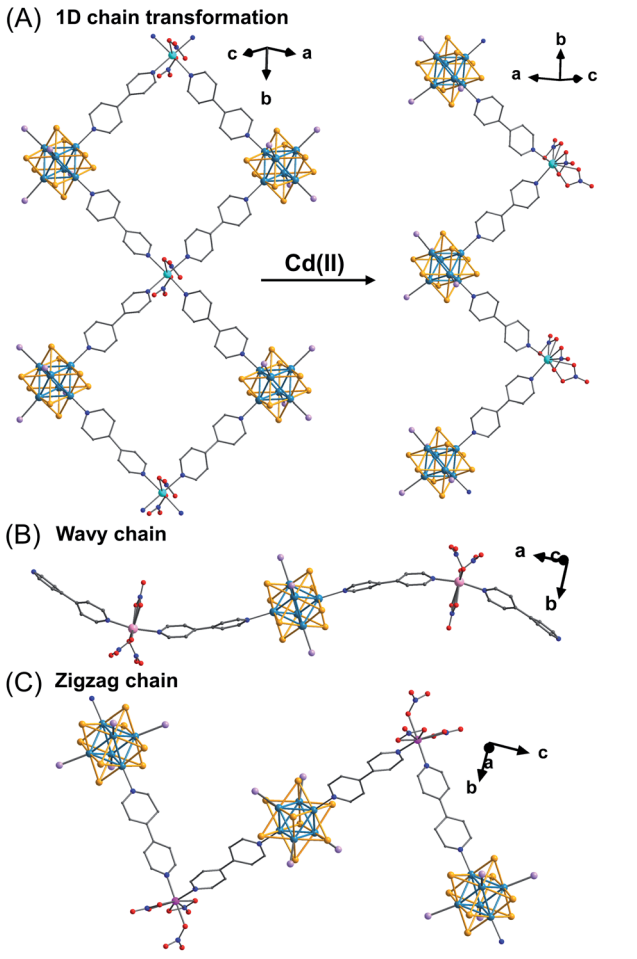

Fig. 9 Schematic representation of the structural transformation of 1D chains based on *cis*-$[Re_6Se_8(PEt_3)_4(bpy)_2]^{2+}$ (A);[50a] a wavy chain (B) and a zigzag chain (C) based on *trans*-$[Re_6Se_8(PEt_3)_4(bpy)_2]^{2+}$.[50b] Color code: Se, orange; O, red; N, blue; P, lavender; C, grey; Cd, sky blue; Co, rose; Zn, pink; Re, navy blue.

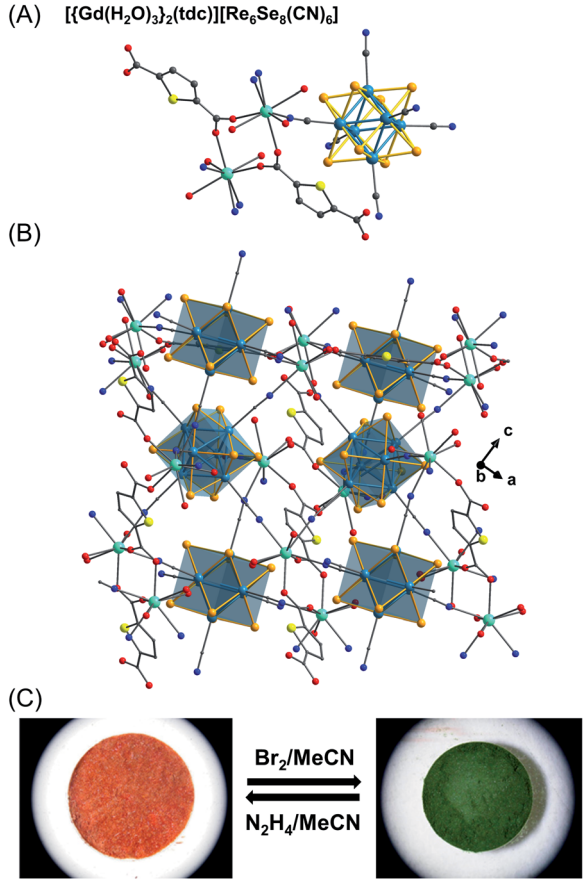

Fig. 10 Part of the asymmetric unit linked by Gd, tdc, and Re_6Se_8 clusters in the MOF material $[\{Gd(H_2O)_3\}_2(tdc)][Re_6Se_8(CN)_6]$ (A) and schematic representation of the crystal packing (B).[51] Color code: Se, orange; O, red; N, blue; C, grey; Gd, light blue; Re, navy blue. Color change of the reversible oxidation and reduction for the bulk material (C) (reproduced from ref. 51 with permission from American Chemical Society, copyright 2018).

studies that have shown that new materials can be built from these clusters.[10]

Among the many possible clusters, Re_6Q_8 is one of the most studied because of its structural stability and intriguing physical properties. Since Long *et al.* discovered a general method to isolate soluble $[Re_6Q_8]^{2+}$ clusters *via* a solid-state route in 1996, materials generated from this hexanuclear rhenium chalcogenide cluster have been rapidly developed.[49] For instance, combining the linker-capped cluster *cis*-$[Re_6Se_8(PPh_3)_4(bpy)_2]^{2+}$ with Cd^{2+} in a 1 : 1 (molar) ratio results in a 1D chain of corner sharing squares (Fig. 9A left). Adding excess Cd^{2+} triggers a further transformation into zigzag chains with denser packing (Fig. 9A right). This transformation suggests an equilibrium between the two structures dependent on the concentration of Cd^{2+}. Similarly, employing *trans*-$[Re_6Se_8(PEt_3)_4(bpy)_2]^{2+}$ as a dipyridyl ligand for coordination with M^{2+} ions (M = Co, Cd, Zn) results in a series of 1D Re_6Se_8-based coordination chains. These chains adopt different configurations such as a wavy arrangement for Cd^{2+} or Co^{2+} (Fig. 9B) or a zigzag chain for Zn^{2+} (Fig. 9C).[50]

Besides these 1D chains, two novel types of 3D porous MOFs have been reported using $[Re_6Se_8(CN)_6]^{4-}$, Gd^{3+}, and dicarboxylate linkers in a three-component framework.[51] These materials exhibit trigonal symmetry which can be viewed as 1D chains of $[\{Gd(H_2O)_3\}_2(L)]^{4+}$ (L = furan-2,5-dicarboxylate, fdc; thiophene-2,5-dicarboxylate, tdc) being extended to three dimensions by the $[Re_6Se_8(CN)_6]^{4-}$ clusters. The SXRD structure of $[\{Gd(H_2O)_3\}_2(tdc)][Re_6Se_8(CN)_6]$ is shown in Fig. 10A and B and serves as a typical example. After activation under vacuum, these porous materials exhibit high volumetric CO_2 uptake (4.18 mmol mL^{-1} at 298 K), comparable with the highest values for MOF materials (*i.e.,* Mg–MOF 74, 2.92 mmol mL^{-1}; HKUST-1, 4.91 mmol mL^{-1}), and remarkable CO_2/N_2 selectivity with a factor of 400 at a total pressure of 1 bar at room temperature. Furthermore, reversible chemical redox events are observed along with color changes and a luminescence response in the red region upon treatment with Br_2/N_2H_4 (Fig. 10C). These findings demonstrate how the properties of these chalcogenide-based clusters can be leveraged in multifunctional materials for gas separation and chemical sensors.

Inspired by the rich chemistry of Re_6Se_8 clusters, a series of differentially and directionally substituted superatoms $Co_6Se_8(CO)_x(PR_3)_{(6-x)}$ have been developed by Champsaur *et al.* Linking two or three clusters with 1,4-phenylenediisocyanide results in the isolation of diatomic and linear triatomic molecules with rich electrochemical profiles that make them ideal for incorporation into redox-switchable frameworks.[52] In order to integrate this type of building block into a solid-state assembly, Champsaur *et al.* functionalized the phosphine ligands of the molecular clusters with carboxylate groups in the precursor $Co_6Se_8[PEt_2(4\text{-}C_6H_4COOH)]_6$ (Fig. 11E). Solvothermal reaction with Zn^{2+} ions leads to a trigonal 3D crystalline solid (Trig 3D, Fig. 11A) or a tetragonal 2D crystalline solid (Tet 2D) if additional HCl is added during the synthesis.[53] While the structure of Trig 3D is a complicated network in which each $\{Co_6Se_8[PEt_2(4\text{-}C_6H_4COO)]_6\}^{6-}$ cluster is coordinated to six unusual

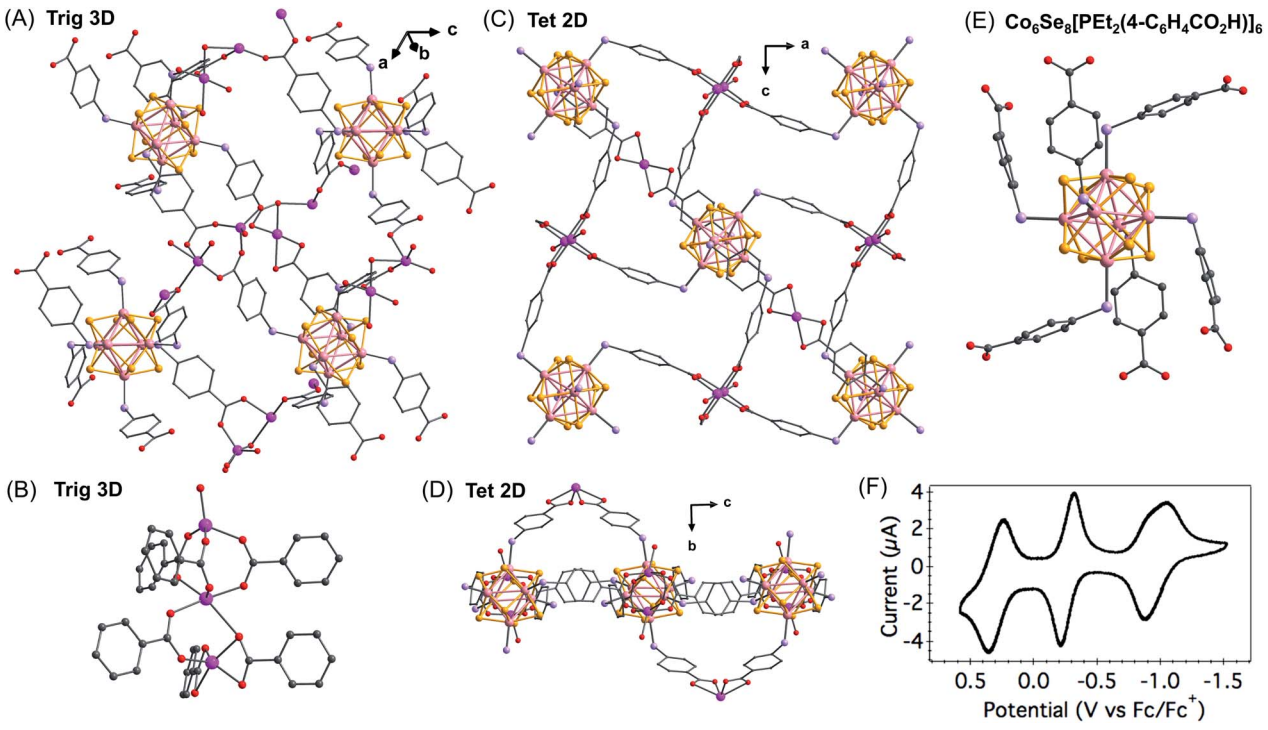

Fig. 11 Partial connection view of Co_6Se_8 clusters and Zn(II) in 3D network Trig 3D (A), structure of tri-Zn clusters (B); views of 2D network Tet 2D along the *b* direction (C), and *c* direction (D); Co_6Se_8 cluster capped with 4-(diethylphosphine)benzoic acid as a building block (E); solid-state cyclic voltammogram of exfoliated Tet 2D sheet (F) (reproduced from ref. 53 with permission from American Chemical Society, copyright 2017).[53] Color code: Se, orange; O, red; P, lavender; C, grey; Zn, pink; Co, rose.

trinuclear Zn nodes (Fig. 11B), Tet 2D is a stacked 2D material in which each layer is a square of Co_6Se_8 clusters bonded to four Zn–carboxylate paddlewheels in the plane (Fig. 11C). In the direction normal to the sheet, two axial carboxylate ligands coordinate an additional Zn^{2+} ion forming bent bridges between neighboring cores above or below the plane (Fig. 11D). Tet 2D can be chemically exfoliated to yield ultrathin, soluble sheets and cyclic voltammetry reveals that the redox properties of the Co_6Se_8 cores are preserved (Fig. 11F). In addition, a novel phosphine stabilized Co_6S_8 molecular cluster formulated as $Co_6S_8(PTA)_6\cdot 4HCl$ (PTA = 1,3,5-triaza-7-phosphaadamantane) has recently been reported as a candidate for redox flow batteries due to its air stability, water solubility, and redox activity. It has been further assembled into a 3D CP with Cu_4I_4 SBUs linked by cage-like PTA units resulting in a semiconducting material with an optical band gap of 1.59 eV.[54] Thus, this class of extended solids also shows potential applications in energy storage.

(e) Coordination polymers based on Mo/W–Cu–S clusters. Discrete Mo(W)–Cu(Ag)–S clusters were investigated starting in the early 1990s, initially motivated as models of enzymatic active sites such as the iron–molybdenum cofactor (FeMoco) and the P^N-cluster of nitrogenase which contain $[MoFe_7S_9]$ and $[Fe_8S_9]$ clusters respectively as well as the heterobimetallic active site of Mo–Cu CODH.[55] An extensive library of stable molecular Mo(W)–M′–S(Se) (M′ = Fe, Cu, Ag, Au, and others) clusters have been synthesized and display notable properties and applications as third-order NLO materials, catalysts, adsorption materials, and sensors.[56] These clusters have therefore also been used as building blocks for the construction of supramolecular assemblies and CPs. Among them, cluster-based coordination oligomers and polymers from Mo(W)–Cu–S precursors with various geometries have been extensively studied by Lang and other groups.[57]

Due to their extensive delocalization and conjugation, Mo(W)–Cu–S compounds are promising third-order NLO materials. A number of extended materials for this targeted application have been described using a preformed cubane-like cluster $[PPh_4][(\eta^5\text{-}C_5Me_5)MoS_3(CuX)_3]$ (X = Br, NCS) and multitopic pyridyl-based ligands, including a family of 1D chains with single, double, triple, and quadruple strands, 2D honeycomb and brick-wall networks, and a 3D adamantane-like network.[58]

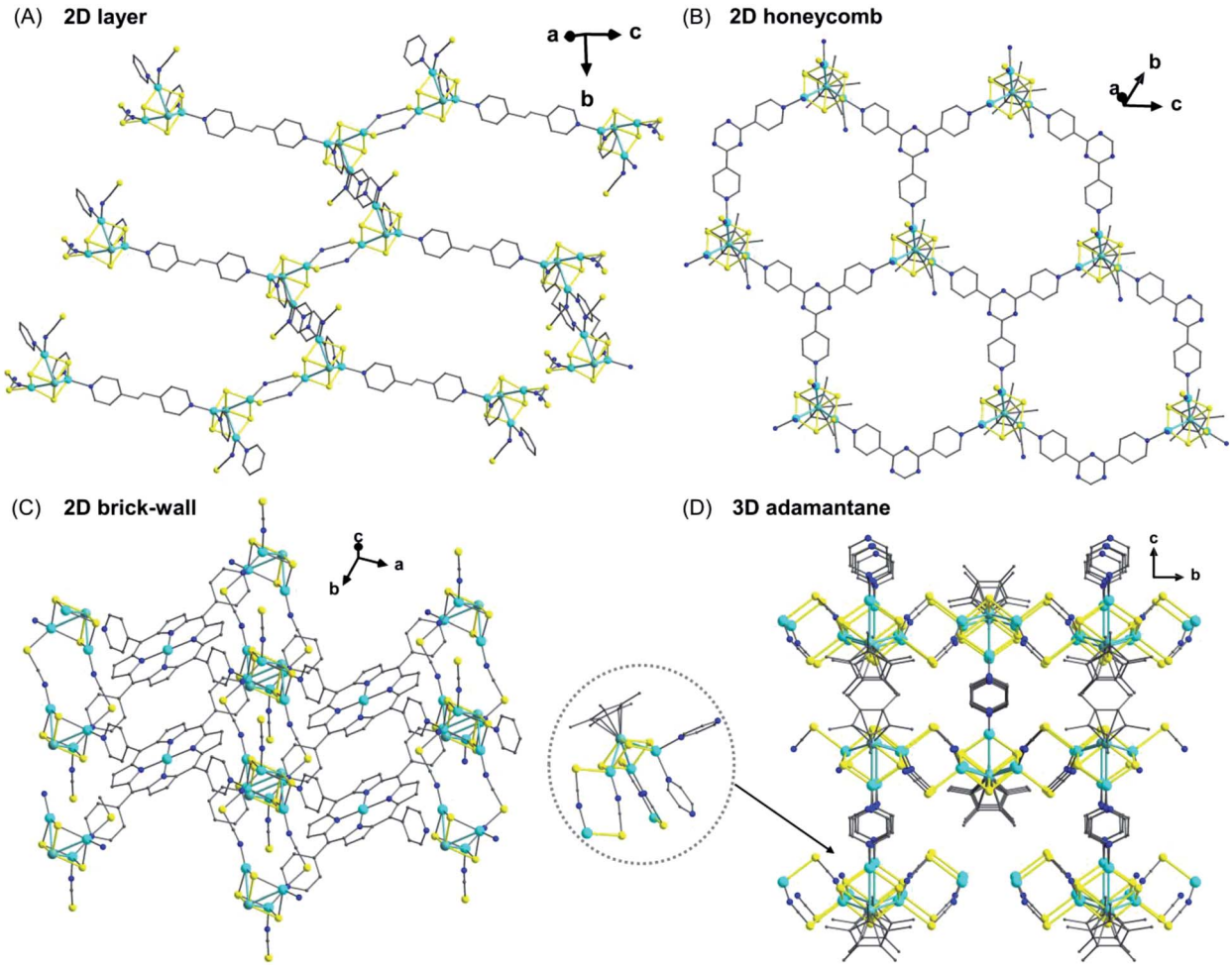

Fig. 12 Perspective view of a 2D layered network based on $[(\eta^5\text{-}C_5Me_5)MoS_3(CuNCS)_3]$ clusters connected by bpea (A); a honeycomb 2D (6,3) network connected by tpt (B); a 2D brick-wall like network connected by H_2tpyp (C); a 3D adamantane like framework connected by 1,4-pyz (D).[58a] Color code: S, yellow; N, blue; C, grey; Cu, sky blue; Mo, light green. η^5-C_5Me_5 in (A) and (C) have been omitted for clarity.

An interesting observation from these results is that the symmetries of the multitopic ligands can essentially dictate the topology of the final polymers. For instance, reacting the cluster $[PPh_4][(\eta^5\text{-}C_5Me_5)MoS_3(CuNCS)_3]$ with bpea (C_s symmetry) gives rise to a 2D layered network in which the cluster cores serve as both T-shaped three-connecting nodes and as angular two-connecting nodes (Fig. 12A). Solid-state reactions of the clusters with 2,4,6-tri(4-pyridyl)-1,3,5-triazine (tpt) (D_{3h} symmetry) affords a honeycomb 2D (6,3) network in which each cluster core serves as a trigonal-planar three-connecting node (Fig. 12B). Using 5,10,15,20-tetra(4-pyridyl)-21*H*,23*H*-porphyrin (H_2tpyp) (D_{4h} symmetry) gives rise to an unusual 2D brick-wall like network where each cluster core acts as a T-shaped three-connecting node (Fig. 12C). On the other hand, using pyrazine (pyz) (D_{2h} symmetry) surprisingly results in a 3D adamantane-like framework with symmetrical tetrahedral connections for the cluster cores (Fig. 12D).[58a]

However, the NLO performance of these materials did not show marked improvement when compared to the cluster-based molecules mostly because of the weak interaction of the pyridyl ligands with the clusters. In contrast, assembling a nest-shaped cluster of $[Et_4N]_2[MoOS_3(CuCN)]$ into 2D (4,4) networks with different equivalents of Cu(I), where cyanide ligands form the bridges, results in a significant increase in NLO performance.[57a] These findings suggest that, aside from assembly effects, the character of the linkers such as charge and bonding can determine the photo-activity of these materials as well.

In addition to the cubane-like clusters mentioned above, ligand substitution of the saddle-shaped $[Et_4N]_4[WS_4Cu_4I_6]$ cluster with bpy affords an unusual 3D porous CP.[57b] The resulting polymer contains an interpenetration of the four independent diamond nets—two $[WS_4Cu_4(bpy)_4]^{2+}$ cationic frameworks and two $[WS_4Cu_4I_4(bpy)_2]^{2-}$ anionic networks. The cationic cluster is coordinated by four pairs of bridging bpy ligands (Fig. 13A) and extends to four crystallographically equivalent clusters that lie at the corners of a distorted tetrahedron, while the anionic cluster (Fig. 13B) retains four iodide ions and further coordinates to four bridging bpy ligands linked to four equivalent clusters that lie at the vertices of a distorted tetrahedron. Beyond these unusual topologies, this $[WS_4Cu_4]$ cluster-based MOF is capable of selectively absorbing iodine and the absorption process is associated with a single-crystal to single-crystal transformation. Fig. 13C shows the phase of the anionic network after I_2 loading. An unusual Cu–I–I–I–Cu bridge that runs parallel to the bpy bridge was discovered in the I_2-loaded phase. This result suggests that these clusters can be functionalized and that unique chemical reactions between guests and clusters can enable applications as sensors or absorbents.

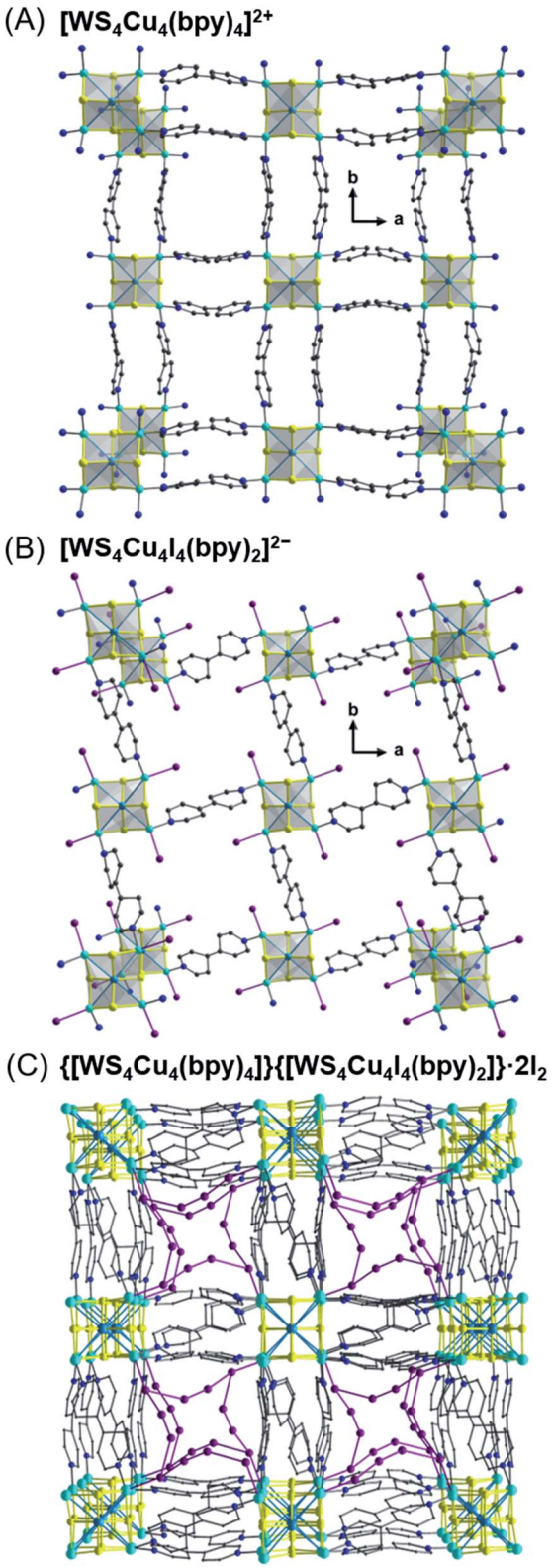

Fig. 13 Representation of the $[WS_4Cu_4(bpy)_4]^{2+}$ cationic framework (A) and the $[WS_4Cu_4I_4(bpy)_2]^{2-}$ anionic network (B); a single channel after absorbing guest I_2 molecules (C).[57b] Color code: S, yellow; N, blue; C, grey; Zn, pink; Cu, sky blue; W, light green; I, dark purple.

Challenges with using heavy chalcogenide-transition metal clusters as building blocks

The above examples clearly demonstrate that heavy-chalcogenide based SBUs have exciting properties that make

their inclusion into CPs attractive. Nevertheless, there are fewer examples of heavy chalcogenide-based SBUs than those based on O or N. As such, it is worthwhile to consider the potential challenges associated with using heavy-chalcogenide based SBUs.

1. Instability of clusters and heavy chalcogenide-based ligands

Many of the clusters and precursors described above are not amenable to classic solvothermal synthesis and require more complicated handling such as air- and water-free conditions. For example, unlike carboxylic acids which form the key ligating functionality in many MOF materials, dithiocarboxylic acids are far less stable. Dithiocarboxylic acids with an α-hydrogen atom are prone to double deprotonation and the resulting dianion is highly reactive and can decompose to other by-products.[59] Some thiolate-based ligands, especially mono- and dithiocarboxylates, are hydrolytically unstable and these linkers tend to degrade into carboxylates under solvothermal conditions with adventitious water. Furthermore, many thiolate, sulfide, or selenide based clusters can also be oxidized or hydrolyzed in air.

Even when stable at room temperature, the decomposition of preformed clusters under harsh synthetic conditions is another concern. For instance, during the synthesis of $[NR_4]_2[Fe_4S_4](BDT)_2$, we found that some amount of $[NR_4]_2[Fe_4S_4](SPh)_4$ decomposed into lamellar iron sulfide when heated for more than one week. Further research showed that the speed of degradation was accelerated with additional oxidants.[60]

2. Comparatively poor crystallinity

To date, SXRD and powder XRD are still two of the primary tools for structural determination of CP materials. Additionally, large crystalline domains are beneficial for physical characterization techniques such as four-probe conductivity measurements.[61] Thus, the preparation of crystalline materials is critical to the design, synthesis, and characterization of new CPs. However, a number of metal–organo–chalcogenide polymers, especially metal–dithiolene-based ones,[8b] suffer from rapid precipitation and poor crystallinity. This problem is shared by the chemistry of covalent organic frameworks (COFs), many of which are also linked through strong covalent bonds.[62]

In looking to address this challenge, mechanistic studies on COFs provide two lessons. First, strong covalent bonds can form quickly and irreversibly which prevents the self-correction of miscoordination and defects eventually leading to disorder. Second, for 1D and 2D CPs, interlayer or interchain packings are also important and the irreversible aggregation of soluble oligomers could lead to nanocrystalline powders.[63] Both factors may play similar roles in the crystallization process of metal–organo–chalcogenide materials, considering the similarly high covalency of metal–chalcogenide bonds. Thus, the rational improvement of crystallization conditions is an urgent problem for the development of novel metal heavy-chalcogenide CPs.

3. Poorly understood effect of templating agents

Modulators are commonly used in conventional MOF synthesis to prevent rapid precipitation of amorphous materials by reversibly binding to SBUs during framework growth.[64] In contrast, few templating agents for heavy-chalcogenide frameworks have been reported. Ethylenediamine is a competing ligand frequently used to improve the crystallinity of strong-bonding frameworks.[65] However, one of the main issues is the incomplete replacement of modulators due to the strong binding of these chelating ligands. Incomplete substitution results in undesired products or impurities associated with ethylenediamine coordination. Monocarboxylate ligands, such as benzenecarboxylate, are frequently used as modulators in conventional MOF synthesis, and the monothiolate ligand, benzenethiolate, may be a likely candidate as a modulator for heavy-chalcogenide based materials. However, as shown above, owing to the large size of sulfur atoms, this ligand may bind multiple metal centers yielding other CPs and insoluble by-products instead of soluble intermediates for dynamic exchange with targeted linkers.

In addition to competing modulators, the charged nature of both preformed heavy chalcogenide SBUs and resulting CPs suggests that ion effects in solution may also be important. We found that *in situ* addition of excess lithium trifluoromethanesulfonate dramatically improved the crystallinity of $[NR_4]_2[Fe_4S_4](BDT)_2$ chains. Ionic screening was proposed as a likely mechanism, but the details of ionic effects on nucleation and crystal growth are yet unclear.

In sum, the usage of modulators is a promising synthetic method to control the crystallinity of chalcogenide-rich frameworks, but current agents suffer from impurities and unwanted by-products. In addition, other templating effects such as ionic strength are still poorly understood.

4. Demands on new synthetic methods for desired morphologies and device fabrication

The challenges in generating crystalline phase-pure frameworks subsequently make their detailed characterization difficult. In order to test the intrinsic electronic structures of many CPs, these materials must be fabricated into suitable morphologies or devices such as thin films or transistors. Conventional chemical vapor deposition (CVD) methods,[66] widely used for the synthesis of inorganic 2D materials, are typically not suitable for fabrication of most CPs. Thus, not only are the syntheses of these materials more challenging than traditional CPs, the synthetic conditions must also be carefully tuned to provide tailored morphologies. Currently, liquid–liquid interface growth is widely adopted for the synthesis of thin films[67] and even monolayer MOFs.[68] This and related approaches are promising for the fabrication of functional inorganic organic hybrid materials in the future.

Opportunities for multifunctional mineral-like coordination polymers

Heavy chalcogenide-based clusters are in some ways atomic level units of solid-state transition metal chalcogenides.[69] As

such, CPs built with these clusters as SBUs may be thought of as inorganic–organic mimics of minerals with the added benefits of tunability and porosity. As demonstrated above, transition metal-heavy chalcogenide clusters inherit electrochemical properties and some functions like catalytic activity from their parent minerals. On the other hand, the reassembly of these clusters with organic linkers leads to porous structures and more diverse topologies, far beyond the limited dense solid phases of their all-inorganic congeners. Porous mineral-like CPs potentially also possess unique interactions with hard/soft guest molecules, which may provide new strategies for heavy metal capture and ion conduction. Plus, porous and robust frameworks should also benefit the catalytic performance of embedded clusters by stabilizing unusual geometries and rigidly separating catalytic sites.

The beginning of the 21st century has seen a surge of interest in two-dimensional materials with layered structures, typified by graphene[70] and transition-metal dichalcogenides.[71] Inspired by these in-plane conjugated 2D inorganic materials, a new family of graphene-like 2D metal–organic frameworks has been reported exhibiting high electrical conductivity and porosity.[72] As exemplified by materials in the previous section, 2D π–d conjugated CPs based on metal-bis-dithiolene nodes display record conductivity and even superconductivity.[35a,b] Transition metal chalcogenide clusters as nodes are less developed despite the fact that the combination of the delocalized electronic structure of clusters with highly conjugated linkers could produce a number of new conducting CP families. In addition to conductivity, nanoscale transition metal dichalcogenides (TMDCs) frequently display semiconducting characteristics. As such, these mineral-like CPs are potentially attractive for applications in electronics and photonics.[73] Moreover, the distinct structures and unique chemical properties of both clusters and organic linkers endow these materials with advantages in some applications such as electrochemical energy storage and coupling of conductivity and magnetism.

1. Structural diversity and associated host–guest chemistry

(a) Preformed clusters serve as highly symmetric building blocks. The concept of SBUs was considered a turning point in the discovery of permanently porous MOFs and in launching the field of reticular chemistry.[74] Polynuclear clusters as SBUs play the key role of dictating the structural diversity inherent to MOFs. Recent advances in the synthesis of MOFs with preformed SBUs and linker molecules allow researchers to prepare pure materials in desirable topologies and crystalline forms.[75] For instance, synthesis from discrete metal–oxygen clusters as starting materials, such as $[Zr_6O_4(OH)_4(OMc)_{12}]$ (OMc = methacrylate), $[Fe_3O(O_2CMe)_6(OH)]$, and $Fe^{III}_3O(MeOH)_3$, results in a number of robust and kinetically inert frameworks with predictable topologies.[76] It is reasonable to expect similar advantages from molecular metal sulfide/selenide clusters. Furthermore, the structural diversity of known heavy-chalcogenide clusters may also enable new framework topologies. Most preformed metal–chalcogenide clusters are highly symmetric, as seen in the O_h-symmetric M_6Q_8 clusters, and are therefore naturally suited for "SBU-directed" synthetic approaches which provide the opportunity to template novel porous structures.

(b) Host–guest interactions and applications. Other than gas and solvent absorption, porous MOFs also offer the ability to store charged guests. Chalcogenide-rich CPs, particularly with anionic frameworks, have dramatically different hard/soft interactions with cationic guests compared to traditional MOF materials. This guest preference has potential applications in heavy metal absorption like Hg^{2+} uptake as well as in ion conduction or battery applications with hard ions such as Li^+ (Fig. 14).[77]

A traditional strategy for heavy metal capture has been functionalization of known MOF frameworks with thiol groups.[78] The formation of strong chemical bonds between

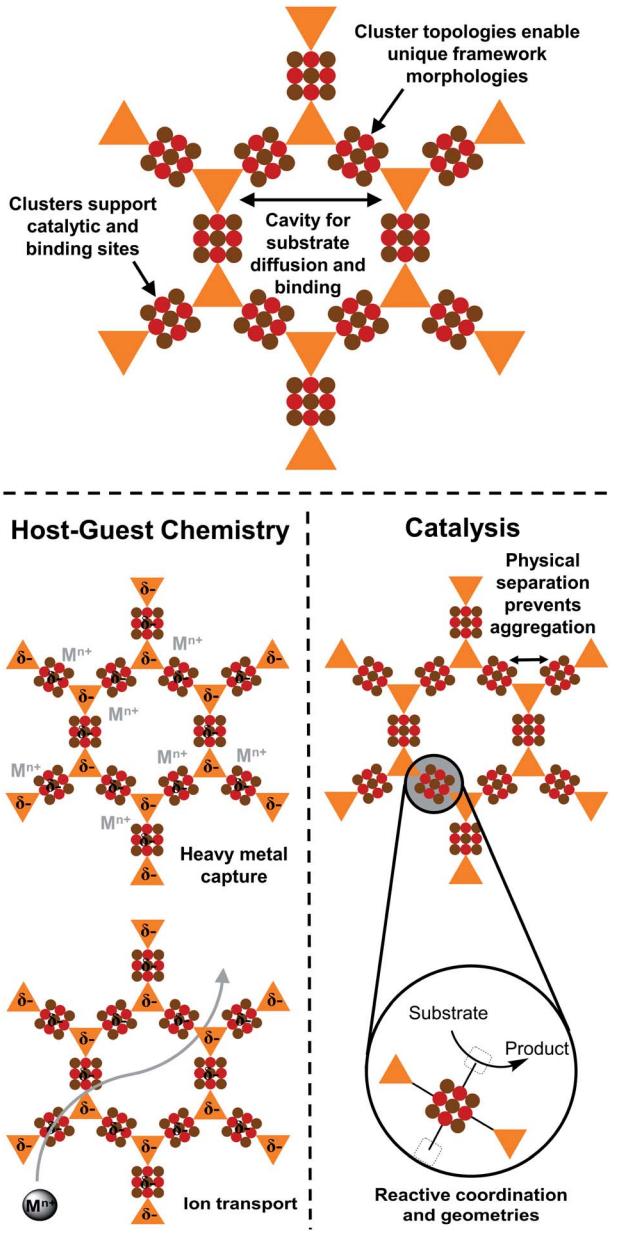

Fig. 14 Potential applications of transition metal-heavy chalcogenide materials in interactions with host cations and cluster-based catalysis.

thiolate and guest metals results in less reversible capture and release, for instance requiring a proton exchange reaction for reversibility.[79] In contrast, the interactions between anionic metal–chalcogenide frameworks and cationic guests should generally be based on electrostatic and non-covalent interactions instead of chemical bond formation, potentially favoring fast and reversible cycling.

In another direction, many MOFs that exhibit high ionic conductivity of alkali and alkaline earth metals are either halide-loaded or have dangling chalcogenide groups.[80,81] Their superionic conductivity is ascribed to an ideal pore size and pore polarity that minimize the activation energy for cation mobility. Despite being less explored in this area, chalcogenide-rich SBUs themselves present the same features and the integration of these SBUs into frameworks could be a new synthetic strategy for highly efficient solid electrolytes.

2. Cluster-based catalysis

(a) Accurate atomic defect engineering. Many heavy chalcogenide clusters support useful chemical transformations and catalysis. For example, in a perspective article, Zheng discussed the activation of small molecules such as acetonitrile and CO by the Lewis acidic cluster core of $[Re_6(\mu_3\text{-}Se)_8]^{2+}$.[82] These chemical transformations suggest that solid-state transition metal clusters embedded in porous frameworks are ideal platforms for similar catalytic applications. To illustrate this potential, we can consider a hypothetical Re_6Se_8-based framework as an example. Inspired by a reported 2D Kagomè $[Re_6Se_8]$-PTA-Ag sheet[83] the proposed platform is shown in Fig. 14 (bottom right), where Re_6Se_8 clusters are integrated into the framework. Two Re sites per cluster would face voids. If these sites were capped by solvent or other weakly bound ligands, they could serve as active catalytic sites. Currently, there has been substantial interest in the development of molecular clusters as models of inorganic minerals in order to accurately control and understand atomic defect formation, and molecular oxide clusters have recently been assembled into coordination networks.[84] Advances in this area suggest exciting possibilities in catalytic materials *via* the reassembly of heavy chalcogenide clusters with organic linkers into new solid-state frameworks. In addition to providing a higher density of catalytic sites compared with homogeneous cluster catalysts, common catalyst deactivation pathways such as aggregation can be avoided as the clusters are rigidly embedded in the framework and have a spatially even distribution.

(b) Addition of catalytic sites *via* post-synthetic modification. Metal–oxygen nodes are widely used as a platform to load single-site active metals for catalysis.[85] For example, Ji, Manna, *et al.* metalated the Zr_{12} SBUs of the MOF Zr_{12}-TPDC with Co affording unsaturated, highly active catalytic sites and a reusable solid catalyst for hydrogenation of various substrates.[6b,c] Similarly, the bridging chalcogenide atoms in many clusters may support additional metal centers *via* analogous post-synthetic modification (Fig. 14). Here too, a similar strategy with molecular clusters has recently been reported with Fe edge sites supported by a Co_6Se_8 cluster.[86] In addition to the unique binding sites provided by these clusters, the rich properties of metal–chalcogenides, such as photo-activity and redox-activity, can potentially enhance catalysis with cooperative effects.[87]

3. Energy storage

Electrochemical energy-storage technologies that power portable electronic devices are ubiquitous in modern life. As such, high-performance energy-storage materials are urgently needed by the growing markets of mobile consumer electronics and electric vehicles. However, the specific capacities and stability of prevalent cathode materials for lithium-ion batteries, such as $LiFePO_4$ and $LiCoO_2$, are fundamentally imposed by their metal-based single electron redox couples.[88] In efforts to surmount this limit, an appealing strategy is promotion of redox activity in metal–organic frameworks.[12,89] The incorporation of metal- and ligand-based redox processes enables redox-active MOFs to achieve theoretical capacities that exceed those of traditional inorganic materials. A key example is the exploration of battery chemistry of semiquinoid-based MOFs by Ziebel *et al.* recently.[90] Indeed, metal–chalcogenide clusters with multiple stable oxidation states are attractive targets as well (Fig. 15). For instance, Li *et al.* reported a reversible Li^+ intercalation process in the hybrid organic/inorganic dimensionally reduced 1D TiS_2(ethylenediamine).[91] Additionally, several 2D and 3D frameworks containing Co_6Se_8 clusters, as discussed above, display reversible redox behavior with potential applications as battery materials.

Outside of battery applications, high surface areas make conductive porous MOFs promising candidates for supercapacitors and particularly pseudocapacitors.[92,93] Pseudocapacitive materials that store charge through battery-like redox processes with fast rates owing to surface reactions offer a pathway to simultaneously achieve high energy density and high power density.[94] TMDCs such as nano-MoS_2 are conventionally considered representative of intrinsic pseudocapacitive materials.[95] Compared to these inorganic congeners, mineral-like CPs are "expanded" by longer organic linkers. The resulting larger voids and higher surface area can ideally allow for efficient mass transport and predominantly surface-centered redox reactions which can benefit charge storage processes. Overall, CPs based on metal–chalcogenide clusters present an attractive target to become a new family of conducting MOFs that meet the twin demands of energy and power density.

4. Coupling conductivity and magnetism

Multifunctional spintronic devices that respond to electrical, magnetic, optical, and chemical stimuli are an area of intense current interest.[96] The development of modern quantum materials, such as topological insulators,[97] is required not only to understand the fundamental properties required for a "second quantum revolution",[98] but also to provide alternatives for traditional logic circuit technology and low-power electronics.[99] Recently, there has been significant interest in spin interactions in conductive MOFs that contain paramagnetic metals or radical ligands.[8a,100] As early as 2013, Wang *et al.* theoretically predicted that the honeycomb framework

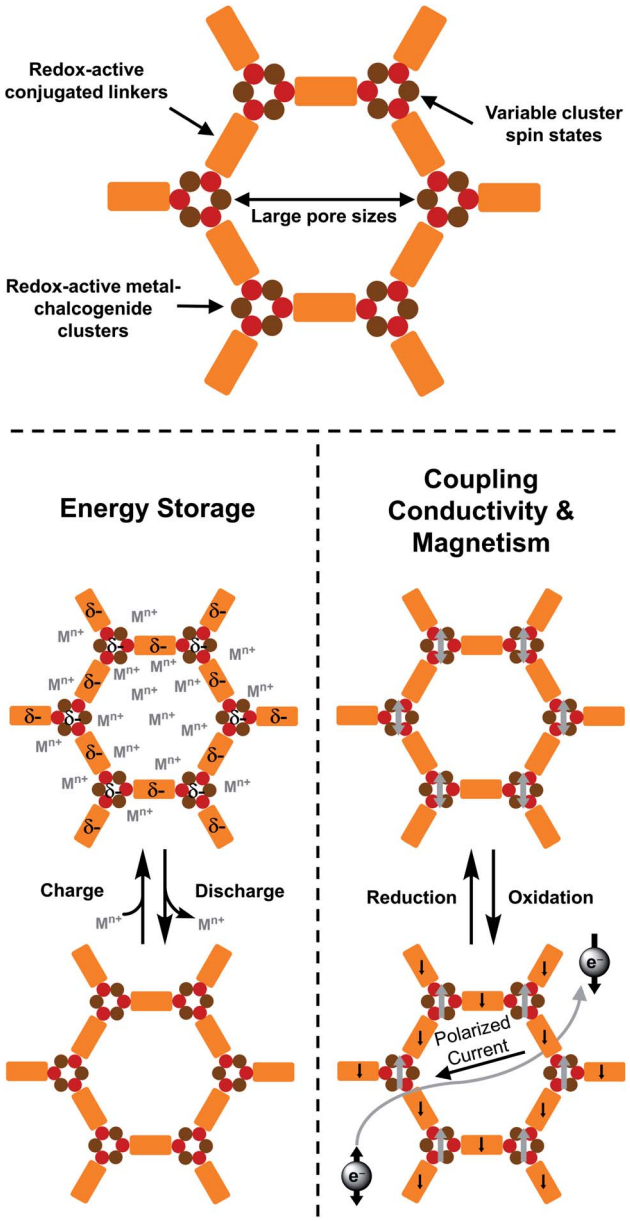

Fig. 15 Proposed applications for transition metal-heavy chalcogenide materials in electrochemical energy storage and coupling conductivity and magnetism.

$Ni_3(BHT)_2$, which was previously synthesized by the Nishihara group, would exhibit nontrivial topological states in both a Dirac band and a flat band.[100a] In 2019, Yang *et al.* modelled the spin interactions in graphene-like conductive MOFs within isolated triphenylene-bridged trinuclear complexes of Cu.[100d] Besides graphene-like frameworks, Liu *et al.* reported the reversible redox switching of both magnetic order and electrical conductivity in manganese benzoquinoid frameworks, suggesting these novel magnetic conductors could have potential applications in spintronic devices.[100e]

In a metal–chalcogenide cluster-based framework with conjugated linkers, the clusters may display high spin ground states and redox-events on cluster SBUs could inject spins into delocalized systems, providing the possibility of coupling conductivity and magnetism (Fig. 15). In addition, compared to current conductive and magnetic MOFs based on first-row transition metals and O-based linkers, CPs that contain heavy metal–chalcogenide clusters could potentially have stronger spin–orbit coupling. Thin films or monolayers of these materials may also exhibit quantum spin Hall effects similar to those observed in monolayer WSe_2/Te_2.[101]

Conclusions

While clusters formed from transition metals and heavy chalcogenides have been known for many years with some examples of CPs reported nearly 40 years ago, these building blocks have still received far less attention than their oxide counterparts in MOF chemistry. This is despite the fact that these clusters have features such as unique geometries, redox and magnetic properties, and hard-soft matching which make them attractive for many applications. While general synthetic protocols for incorporating these clusters into CPs are less well-developed, recent examples illustrate that these promising building blocks can be reliably incorporated into new CP materials. The use of these clusters as nodes therefore offers exciting potential for emerging areas in CP and MOF materials and applications.

Conflicts of interest

There are no conflicts to declare.

Acknowledgements

The authors gratefully acknowledge support for this work from the U.S. Department of Energy, Office of Science, Office of Basic Energy Sciences, under Award No. DE-SC0019215.

Notes and references

1 (*a*) J.-R. Li, R. J. Kuppler and H.-C. Zhou, Selective Gas Adsorption and Separation in Metal–Organic Frameworks, *Chem. Soc. Rev.*, 2009, **38**, 1477–1504; (*b*) H. Furukawa, K. E. Cordova, M. O'Keeffe and O. M. Yaghi, The Chemistry and Applications of Metal–Organic Frameworks, *Science*, 2013, **341**, 1230444; (*c*) Y. Zhang, X. Feng, S. Yuan, J. Zhou and B. Wang, Challenges and Recent Advances in MOF–Polymer Composite Membranes for Gas Separation, *Inorg. Chem. Front.*, 2016, **3**, 896–909; (*d*) G. Maurin, C. Serre, A. Cooper and G. Férey, The New Age of MOFs and of Their Porous-Related Solids, *Chem. Soc. Rev.*, 2017, **46**, 3104–3107.

2 (*a*) K. Sumida, D. L. Rogow, J. A. Mason, T. M. McDonald, E. D. Bloch, Z. R. Herm, T.-H. Bae and J. R. Long, Carbon Dioxide Capture in Metal–Organic Frameworks, *Chem. Rev.*, 2012, **112**, 724–781; (*b*) C. A. Trickett, A. Helal, B. A. Al-Maythalony, Z. H. Yamani, K. E. Cordova and O. M. Yaghi, The Chemistry of Metal–Organic Frameworks for CO_2 Capture, Regeneration and Conversion, *Nat. Rev. Mater.*, 2017, **2**, 17045.

3 (*a*) L. Ma, C. Abney and W. Lin, Enantioselective Catalysis with Homochiral Metal–Organic Frameworks, *Chem. Soc. Rev.*, 2009, **38**, 1248–1256; (*b*) J. Lee, O. K. Farha, J. Roberts, K. A. Scheidt, S. T. Nguyen and J. T. Hupp, Metal–Organic Framework Materials as Catalysts, *Chem. Soc. Rev.*, 2009, **38**, 1450–1459.

4 (*a*) P. Horcajada, R. Gref, T. Baati, P. K. Allan, G. Maurin, P. Couvreur, G. Férey, R. E. Morris and C. Serre, Metal–Organic Frameworks in Biomedicine, *Chem. Rev.*, 2012, **112**, 1232–1268; (*b*) W. Cai, J. Wang, C. Chu, W. Chen, C. Wu and G. Liu, Metal–Organic Framework-Based Stimuli-Responsive Systems for Drug Delivery, *Adv. Sci.*, 2019, **6**, 1801526.

5 (*a*) H. Li, M. Eddaoudi, M. O'Keeffe and O. M. Yaghi, Design and Synthesis of an Exceptionally Stable and Highly Porous Metal–Organic Framework, *Nature*, 1999, **402**, 276–279; (*b*) J. H. Cavka, S. Jakobsen, U. Olsbye, N. Guillou, C. Lamberti, S. Bordiga and K. P. Lillerud, A New Zirconium Inorganic Building Brick Forming Metal Organic Frameworks with Exceptional Stability, *J. Am. Chem. Soc.*, 2008, **130**, 13850–13851.

6 (*a*) K. Manna, P. Ji, Z. Lin, F. X. Greene, A. Urban, N. C. Thacker and W. Lin, Chemoselective Single-Site Earth-Abundant Metal Catalysts at Metal–Organic Framework Nodes, *Nat. Commun.*, 2016, **7**, 12610; (*b*) P. Ji, K. Manna, Z. Lin, A. Urban, F. X. Greene, G. Lan and W. Lin, Single-Site Cobalt Catalysts at New $Zr_8(\mu_2\text{-}O)_8(\mu_2\text{-}OH)_4$ Metal–Organic Framework Nodes for Highly Active Hydrogenation of Alkenes, Imines, Carbonyls, and Heterocycles, *J. Am. Chem. Soc.*, 2016, **138**, 12234–12242; (*c*) P. Ji, K. Manna, Z. Lin, X. Feng, A. Urban, Y. Song and W. Lin, Single-Site Cobalt Catalysts at New $Zr_{12}(\mu_3\text{-}O)_8(\mu_3\text{-}OH)_8(\mu_2\text{-}OH)_6$ Metal–Organic Framework Nodes for Highly Active Hydrogenation of Nitroarenes, Nitriles, and Isocyanides, *J. Am. Chem. Soc.*, 2017, **139**, 7004–7011; (*d*) C. Xu, R. Fang, R. Luque, L. Chen and Y. Li, Functional Metal–Organic Frameworks for Catalytic Applications, *Coord. Chem. Rev.*, 2019, **388**, 268–292.

7 (*a*) L. Sun, M. G. Campbell and M. Dincă, Electrically Conductive Porous Metal–Organic Frameworks, *Angew. Chem., Int. Ed.*, 2016, **55**, 3566–3579; (*b*) L. S. Xie, G. Skorupskii and M. Dincă, Electrically Conductive Metal–Organic Frameworks, *Chem. Rev.*, 2020, DOI: 10.1021/acs.chemrev.9b00766; (*c*) A. E. Thorarinsdottir and T. D. Harris, Metal–Organic Framework Magnets, *Chem. Rev.*, 2020, DOI: 10.1021/acs.chemrev.9b00666.

8 (*a*) R. Dong, Z. Zhang, D. C. Tranca, S. Zhou, M. Wang, P. Adler, Z. Liao, F. Liu, Y. Sun, W. Shi, Z. Zhang, E. Zschech, S. C. B. Mannsfeld, C. Felser and X. Feng, A Coronene-Based Semiconducting Two-Dimensional Metal–Organic Framework with Ferromagnetic Behavior, *Nat. Commun.*, 2018, **9**, 2637; (*b*) T. Kusamoto and H. Nishihara, Zero-, One- and Two-Dimensional Bis(Dithiolato)Metal Complexes with Unique Physical and Chemical Properties, *Coord. Chem. Rev.*, 2019, **380**, 419–439.

9 (*a*) H. Beinert, Iron–Sulfur Clusters: Nature's Modular, Multipurpose Structures, *Science*, 1997, **277**, 653–659; (*b*) B. M. Hoffman, D. Lukoyanov, Z.-Y. Yang, D. R. Dean and L. C. Seefeldt, Mechanism of Nitrogen Fixation by Nitrogenase: The Next Stage, *Chem. Rev.*, 2014, **114**, 4041–4062; (*c*) S. Anantharaj, S. R. Ede, K. Sakthikumar, K. Karthick, S. Mishra and S. Kundu, Recent Trends and Perspectives in Electrochemical Water Splitting with an Emphasis on Sulfide, Selenide, and Phosphide Catalysts of Fe, Co, and Ni: A Review, *ACS Catal.*, 2016, **6**, 8069–8097; (*d*) K. Tanifuji and Y. Ohki, Metal–Sulfur Compounds in N_2 Reduction and Nitrogenase-Related Chemistry, *Chem. Rev.*, 2020, **120**, 5194–5251.

10 (*a*) P. Jena and Q. Sun, Super Atomic Clusters: Design Rules and Potential for Building Blocks of Materials, *Chem. Rev.*, 2018, **118**, 5755–5870; (*b*) N. A. Gadjieva, A. M. Champsaur, M. L. Steigerwald, X. Roy and C. Nuckolls, Dimensional Control of Assembling Metal Chalcogenide Clusters, *Eur. J. Inorg. Chem.*, 2020, **2020**, 1245–1254; (*c*) E. A. Doud, A. Voevodin, T. J. Hochuli, A. M. Champsaur, C. Nuckolls and X. Roy, Superatoms in Materials Science, *Nat. Rev. Mater.*, 2020, **5**, 371–387; (*d*) C. Palencia, K. Yu and K. Boldt, The Future of Colloidal Semiconductor Magic-Size Clusters, *ACS Nano*, 2020, **14**, 1227–1235.

11 B. F. Hoskins and R. Robson, Design and Construction of a New Class of Scaffolding-like Materials Comprising Infinite Polymeric Frameworks of 3D-Linked Molecular Rods. A Reappraisal of the Zinc Cyanide and Cadmium Cyanide Structures and the Synthesis and Structure of the Diamond-Rela, *J. Am. Chem. Soc.*, 1990, **112**, 1546–1554.

12 (*a*) M. Dincă and F. Léonard, Metal–Organic Frameworks for Electronics and Photonics, *MRS Bull.*, 2016, **41**, 854–857; (*b*) L. Wang, Y. Han, X. Feng, J. Zhou, P. Qi and B. Wang, Metal–Organic Frameworks for Energy Storage: Batteries and Supercapacitors, *Coord. Chem. Rev.*, 2016, **307**, 361–381; (*c*) A. E. Baumann, D. A. Burns, B. Liu and V. S. Thoi, Metal–Organic Framework Functionalization and Design Strategies for Advanced Electrochemical Energy Storage Devices, *Commun. Chem.*, 2019, **2**, 86.

13 (*a*) L. Sun, T. Miyakai, S. Seki and M. Dincă, Mn_2(2,5-Disulfhydrylbenzene-1,4-Dicarboxylate): A Microporous Metal–Organic Framework with Infinite $(\text{–Mn–S–})_\infty$ Chains and High Intrinsic Charge Mobility, *J. Am. Chem. Soc.*, 2013, **135**, 8185–8188; (*b*) L. Sun, C. H. Hendon, M. A. Minier, A. Walsh and M. Dincă, Million-Fold Electrical Conductivity Enhancement in Fe_2(DEBDC) *versus* Mn_2(DEBDC) (E = S, O), *J. Am. Chem. Soc.*, 2015, **137**, 6164–6167; (*c*) L. Sun, C. H. Hendon and M. Dincă, Coordination-Induced Reversible Electrical Conductivity Variation in the MOF-74 Analogue Fe_2(DSBDC), *Dalton Trans.*, 2018, **47**, 11739–11743.

14 (*a*) A. Saeki, S. Seki, Y. Koizumi, T. Sunagawa, K. Ushida and S. Tagawa, Increase in the Mobility of Photogenerated Positive Charge Carriers in Polythiophene, *J. Phys. Chem. B*, 2005, **109**, 10015–10019; (*b*) A. Saeki, S. Seki, T. Sunagawa, K. Ushida and S. Tagawa, Charge-Carrier Dynamics in Polythiophene Films Studied by In-Situ Measurement of Flash-Photolysis Time-Resolved Microwave Conductivity (FP-TRMC) and Transient Optical

Spectroscopy (TOS), *Philos. Mag.*, 2006, **86**, 1261–1276; (*c*) A. Saeki, S. Ohsaki, S. Seki and S. Tagawa, Electrodeless Determination of Charge Carrier Mobility in Poly(3-Hexylthiophene) Films Incorporating Perylenediimide as Photoconductivity Sensitizer and Spectroscopic Probe, *J. Phys. Chem. C*, 2008, **112**, 16643–16650.

15 A. Saeki, S. Seki, T. Takenobu, Y. Iwasa and S. Tagawa, Mobility and Dynamics of Charge Carriers in Rubrene Single Crystals Studied by Flash-Photolysis Microwave Conductivity and Optical Spectroscopy, *Adv. Mater.*, 2008, **20**, 920–923.

16 Q. Zhang, B. Li and L. Chen, First-Principles Study of Microporous Magnets M–MOF-74 (M = Ni, Co, Fe, Mn): The Role of Metal Centers, *Inorg. Chem.*, 2013, **52**, 9356–9362.

17 L. Sun, C. H. Hendon, S. S. Park, Y. Tulchinsky, R. Wan, F. Wang, A. Walsh and M. Dincă, Is Iron Unique in Promoting Electrical Conductivity in MOFs?, *Chem. Sci.*, 2017, **8**, 4450–4457.

18 B. J. Holliday and T. M. Swager, Conducting Metallopolymers: The Roles of Molecular Architecture and Redox Matching, *Chem. Commun.*, 2005, 23–36.

19 X.-S. Wang, S. Ma, D. Sun, S. Parkin and H.-C. Zhou, A Mesoporous Metal–Organic Framework with Permanent Porosity, *J. Am. Chem. Soc.*, 2006, **128**, 16474–16475.

20 M. Dincă, A. Dailly, Y. Liu, C. M. Brown, D. A. Neumann and J. R. Long, Hydrogen Storage in a Microporous Metal–Organic Framework with Exposed Mn^{2+} Coordination Sites, *J. Am. Chem. Soc.*, 2006, **128**, 16876–16883.

21 (*a*) B. F. Abrahams, M. G. Haywood and R. Robson, $[Co(NH_3)_6]_3[Cu_4(OH)(CO_3)_8]\cdot 2H_2O$ – a New Carbonato–Copper(ii) Anion Stabilized by Extensive Hydrogen Bonding, *Chem. Commun.*, 2004, **4**, 938–939; (*b*) S. Das, H. Kim and K. Kim, Metathesis in Single Crystal: Complete and Reversible Exchange of Metal Ions Constituting the Frameworks of Metal–Organic Frameworks, *J. Am. Chem. Soc.*, 2009, **131**, 3814–3815; (*c*) X.-M. Zhang, J. Lv, F. Ji, H.-S. Wu, H. Jiao and P. v. R. Schleyer, A Perfectly Square-Planar Tetracoordinated Oxygen in a Tetracopper Cluster-Based Coordination Polymer, *J. Am. Chem. Soc.*, 2011, **133**, 4788–4790; (*d*) Q. Chen, W. Xue, J. Bin Lin, Y. S. Wei, Z. Yin, M. H. Zeng, M. Kurmoo and X. M. Chen, Windmill $Co_4\{Co_4(M_4\text{-}O)\}$ with 16 Divergent Branches Forming a Family of Metal–Organic Frameworks: Organic Metrics Control Topology, Gas Sorption, and Magnetism, *Chem.–Eur. J.*, 2016, **22**, 12088–12094; (*e*) Q.-H. Meng, J.-L. Liu, X. Long, S. Zhang and Y. Quan, A Porous the-Type Metal–Organic Framework Based on $[Mn_4Cl]^{7+}$ Clusters for Selective Gas Sorption, *Inorg. Chem. Commun.*, 2017, **79**, 46–49.

22 H. Yang, M. Luo, Z. Wu, W. Wang, C. Xue and T. Wu, A Semiconducting Metal–Chalcogenide–Organic Framework with Square-Planar Tetra-Coordinated Sulfur, *Chem. Commun.*, 2018, **54**, 11272–11275.

23 (*a*) M. Xue, G. Zhu, Q. Fang, X. Guo and S. Qiu, Solvothermal Synthesis, Structure and Magnetism of Two Novel 3D Metal–Organic Frameworks Based on Infinite Helical Mn–O–C Rod-Shaped Building Units, *J. Mol. Struct.*, 2006, **796**, 165–171; (*b*) Y. Fu, J. Su, S. Yang, G. Li, F. Liao, M. Xiong and J. Lin, Syntheses, Structures and Magnetic Properties of Mn(ii), Co(ii) and Ni(ii) Metal–Organic Frameworks Constructed from 1,3,5-Benzenetricarboxylate and Formate Ligands, *Inorg. Chim. Acta*, 2010, **363**, 645–652.

24 (*a*) B. Krebs and G. Henkel, Transition-Metal Thiolates: From Molecular Fragments of Sulfidic Solids to Models for Active Centers in Biomolecules, *Angew. Chem., Int. Ed. Engl.*, 1991, **30**, 769–788; (*b*) J. Han and D. Coucouvanis, Synthesis and Structure of Singly Bridged and Doubly Bridged $[MoFe_3S_4]$ Double Cubanes with Bidentate Phosphine Ligands, *Inorg. Chem.*, 2002, **41**, 2738–2746; (*c*) H. N. Kagalwala, E. Gottlieb, G. Li, T. Li, R. Jin and S. Bernhard, Photocatalytic Hydrogen Generation System Using a Nickel-Thiolate Hexameric Cluster, *Inorg. Chem.*, 2013, **52**, 9094–9101.

25 (*a*) F. Tuna, C. A. Smith, M. Bodensteiner, L. Ungur, L. F. Chibotaru, E. J. L. McInnes, R. E. P. Winpenny, D. Collison and R. A. Layfield, A High Anisotropy Barrier in a Sulfur-Bridged Organodysprosium Single-Molecule Magnet, *Angew. Chem., Int. Ed.*, 2012, **51**, 6976–6980; (*b*) S.-D. Han, X.-H. Miao, S.-J. Liu and X.-H. Bu, A Series of Cobalt and Nickel Clusters Based on Thiol-Containing Ligands Accompanied by In Situ Ligand Formation, *Dalton Trans.*, 2015, **44**, 560–567.

26 (*a*) D. Fenske and A. Fischer, New Selenolato-Bridged Clusters of Iron and Nickel; the Structures of $[Fe_{12}(SePh)_{24}]$ and $[Na_2(POPh_3)_6][Ni_{20}Se_{12}(SeMe)_{10}]$, *Angew. Chem., Int. Ed.*, 1995, **34**, 307–309; (*b*) C. Zhang, S. Takada, M. Kölzer, T. Matsumoto and K. Tatsumi, Nickel(ii) Thiolate Complexes with a Flexiblecyclo-$\{Ni_{10}S_{20}\}$ Framework, *Angew. Chem., Int. Ed.*, 2006, **45**, 3768–3772; (*c*) H. Jiang, T. Sheng, S. Bai, S. Hu, X. Wang, R. Fu, P. Yu and X. Wu, Unusual C–S Bond Cleavage in Hydro(Solvo)Thermal Reaction That Induces Two Novel Nickel Thiolates: The Crown $[Ni_{16}(edt)_8S_9(S_2)]^{4-}$ with an Unprecedented 12-Membered Ring System and the Cage like $[Ni_{13}(edt)_8S_4(S_2)_2]^{2-}$ with Two Distorted C, *Inorg. Chem.*, 2013, **52**, 12305–12307.

27 (*a*) J. Kim, B. Chen, T. M. Reineke, H. Li, M. Eddaoudi, D. B. Moler, M. O'Keeffe and O. M. Yaghi, Assembly of Metal–Organic Frameworks from Large Organic and Inorganic Secondary Building Units: New Examples and Simplifying Principles for Complex Structures, *J. Am. Chem. Soc.*, 2001, **123**, 8239–8247; (*b*) A. J. Howarth, A. W. Peters, N. A. Vermeulen, T. C. Wang, J. T. Hupp and O. K. Farha, Best Practices for the Synthesis, Activation, and Characterization of Metal–Organic Frameworks, *Chem. Mater.*, 2017, **29**, 26–39.

28 Y. Zhao, M. Hong, Y. Liang, R. Cao, W. Li, J. Weng and S. Lu, A Paramagnetic Lamellar Polymer with a High Semiconductivity, *Chem. Commun.*, 2001, **11**, 1020–1021.

29 N. Yuan, C. Tian, T. Sheng, S. Hu and X. Wu, New Magnetic Nickel(ii)-Thiolate Cluster-Based Coordination Polymer

Constructed from 2-Mercaptonicotinic Acid, *Cryst. Growth Des.*, 2018, **18**, 2667–2671.

30 A. Eichhöfer and S. Lebedkin, 1D and 3D Polymeric Manganese(II) Thiolato Complexes: Synthesis, Structure, and Properties of $_\infty{}^3[Mn_4(SPh)_8]$ and $_\infty{}^1[Mn(SMes)_2]$, *Inorg. Chem.*, 2018, **57**, 602–608.

31 (*a*) M. Bochmann, A. K. Powell and X. Song, Synthesis and Characterisation of Manganese(II) Chalcogenolato Complexes. Crystal and Molecular Structure of $[\{Mn(\mu\text{-}SeC_6H_2Me_3\text{-}2,4,6)_2\}_\infty]$, *J. Chem. Soc., Dalton Trans.*, 1995, **10**, 1645–1648; (*b*) A. Eichhöfer, G. Buth, F. Dolci, K. Fink, R. A. Mole and P. T. Wood, Homoleptic 1-D Iron Selenolate Complexes—Synthesis, Structure, Magnetic and Thermal Behavior of $_\infty{}^1[Fe(SeR)_2]$ (R = Ph, Mes), *Dalton Trans.*, 2011, **40**, 7022–7032; (*c*) A. Eichhöfer and G. Buth, Polymeric Cobalt(II) Thiolato Complexes – Syntheses, Structures and Properties of $_\infty{}^1[Co(SMes)_2]$ and $_\infty{}^1[Co(SPh)_2NH_3]$, *Dalton Trans.*, 2016, **45**, 17382–17391; (*d*) A. Eichhöfer and G. Buth, 1-D Polymeric Iron(II) Thiolato Complexes: Synthesis, Structure, and Properties of $_\infty{}^1[[Fe(SR)_2]$ (R = Ph, Mes), $_\infty{}^1[Fe(NH_3)(SPh)(\mu\text{-}SPh)]$ and $_\infty{}^1[(\mu\text{-}Sph)Fe(NH_3)_2(\mu\text{-}SPh)_2Fe(\mu\text{-}SPh)]$, *Eur. J. Inorg. Chem.*, 2019, **5**, 639–646.

32 (*a*) J. B. Goodenough, Theory of the Role of Covalence in the Perovskite-Type Manganites [La, M(II)]MnO_3, *Phys. Rev.*, 1955, **100**, 564–573; (*b*) J. B. Goodenough, An Interpretation of the Magnetic Properties of the Perovskite-Type Mixed Crystals $La_{1-x}Sr_xCoO_{3-\lambda}$, *J. Phys. Chem. Solids*, 1958, **6**, 287–297; (*c*) J. Kanamori, Superexchange Interaction and Symmetry Properties of Electron Orbitals, *J. Phys. Chem. Solids*, 1959, **10**, 87–98.

33 (*a*) D. Cave, J.-M. Gascon, A. D. Bond, S. J. Teat and P. T. Wood, Layered Metal Organosulfides: Hydrothermal Synthesis, Structure and Magnetic Behavior of the Spin-Canted Magnet $Co(1,2\text{-}(O_2C)(S)C_6H_4)$, *Chem. Commun.*, 2002, **10**, 1050–1051; (*b*) Y. Ling, H. Chen, J. Zhou, K. Tao, S. Zhao, X. Yu and L. Han, Metal-Organosulfide Coordination Polymer Nanosheet Array as a Battery-Type Electrode for an Asymmetric Supercapacitor, *Inorg. Chem.*, 2020, **59**, 7360–7369.

34 S. M. Humphrey, R. A. Mole, M. McPartlin, E. J. L. McInnes and P. T. Wood, Isolated Magnetic Clusters of Co(II) and Ni(II) within 3-Dimensional Organic Frameworks of 6-Mercaptonicotinic Acid: Unique Structural Topologies Based on Selectivity for Hard and Soft Coordination Environments, *Inorg. Chem.*, 2005, **44**, 5981–5983.

35 (*a*) X. Huang, P. Sheng, Z. Tu, F. Zhang, J. Wang, H. Geng, Y. Zou, C.-a. Di, Y. Yi, Y. Sun, W. Xu and D. Zhu, Two-Dimensional π–d Conjugated Coordination Polymer with Extremely High Electrical Conductivity and Ambipolar Transport Behavior, *Nat. Commun.*, 2015, **6**, 7408–7416; (*b*) X. Huang, S. Zhang, L. Liu, L. Yu, G. Chen, W. Xu and D. Zhu, Superconductivity in a Copper(II)-Based Coordination Polymer with Perfect Kagomè Structure, *Angew. Chem., Int. Ed.*, 2018, **57**, 146–150; (*c*) Y. Cui, J. Yan, Z. Chen, J. Zhang, Y. Zou, Y. Sun, W. Xu and D. Zhu, $[Cu_3(C_6Se_6)]_n$: The First Highly Conductive 2D π–d Conjugated Coordination Polymer Based on Benzenehexaselenolate, *Adv. Sci.*, 2019, **6**, 1802235–1802240.

36 (*a*) H. D. Selby, B. K. Roland and Z. Zheng, Ligand-Bridged Oligomeric and Supramolecular Arrays of the Hexanuclear Rhenium Selenide Clusters-Exploratory Synthesis, Structural Characterization, and Property Investigation, *Acc. Chem. Res.*, 2003, **36**, 933–944; (*b*) S. C. Lee, W. Lo and R. H. Holm, Developments in the Biomimetic Chemistry of Cubane-Type and Higher Nuclearity Iron–Sulfur Clusters, *Chem. Rev.*, 2014, **114**, 3579–3600.

37 M. Verdaguer and A. N. Gleizes, Magnetism: Molecules to Build Solids, *Eur. J. Inorg. Chem.*, 2020, **2020**, 723–731.

38 (*a*) T. F. Jaramillo, K. P. Jorgensen, J. Bonde, J. H. Nielsen, S. Horch and I. Chorkendorff, Identification of Active Edge Sites for Electrochemical H_2 Evolution from MoS_2 Nanocatalysts, *Science*, 2007, **317**, 100–102; (*b*) Y. Li, H. Wang, L. Xie, Y. Liang, G. Hong and H. Dai, MoS_2 Nanoparticles Grown on Graphene: An Advanced Catalyst for the Hydrogen Evolution Reaction, *J. Am. Chem. Soc.*, 2011, **133**, 7296–7299; (*c*) H. I. Karunadasa, E. Montalvo, Y. Sun, M. Majda, J. R. Long and C. J. Chang, A Molecular MoS_2 Edge Site Mimic for Catalytic Hydrogen Generation, *Science*, 2012, **335**, 698–702; (*d*) M.-R. Gao, M. K. Y. Chan and Y. Sun, Edge-Terminated Molybdenum Disulfide with a 9.4 Å Interlayer Spacing for Electrochemical Hydrogen Production, *Nat. Commun.*, 2015, **6**, 7493.

39 (*a*) D. Recatalá, R. Llusar, A. L. Gushchin, E. A. Kozlova, Y. A. Laricheva, P. A. Abramov, M. N. Sokolov, R. Gómez and T. Lana-Villarreal, Photogeneration of Hydrogen from Water by Hybrid Molybdenum Sulfide Clusters Immobilized on Titania, *ChemSusChem*, 2015, **8**, 148–157; (*b*) P. D. Tran, T. V. Tran, M. Orio, S. Torelli, Q. D. Truong, K. Nayuki, Y. Sasaki, S. Y. Chiam, R. Yi, I. Honma, J. Barber and V. Artero, Coordination Polymer Structure and Revisited Hydrogen Evolution Catalytic Mechanism for Amorphous Molybdenum Sulfide, *Nat. Mater.*, 2016, **15**, 640–646.

40 Z. Ji, C. Trickett, X. Pei and O. M. Yaghi, Linking Molybdenum–Sulfur Clusters for Electrocatalytic Hydrogen Evolution, *J. Am. Chem. Soc.*, 2018, **140**, 13618–13622.

41 (*a*) H. Beinert, Iron–Sulfur Proteins: Ancient Structures, Still Full of Surprises, *JBIC, J. Biol. Inorg. Chem.*, 2000, **5**, 2–15; (*b*) D. C. Johnson, D. R. Dean, A. D. Smith and M. K. Johnson, Structure, Function, and Formation of Biological Iron–Sulfur Clusters, *Annu. Rev. Biochem.*, 2005, **74**, 247–281.

42 (*a*) P. Venkateswara Rao and R. H. Holm, Synthetic Analogues of the Active Sites of Iron–Sulfur Proteins, *Chem. Rev.*, 2004, **104**, 527–559; (*b*) R. H. Holm and W. Lo, Structural Conversions of Synthetic and Protein-Bound Iron–Sulfur Clusters, *Chem. Rev.*, 2016, **116**, 13685–13713.

43 N. E. Horwitz, J. Xie, A. S. Filatov, R. J. Papoular, W. E. Shepard, D. Z. Zee, M. P. Grahn, C. Gilder and J. S. Anderson, Redox-Active 1D Coordination Polymers of

Iron–Sulfur Clusters, *J. Am. Chem. Soc.*, 2019, **141**, 3940–3951.

44 (*a*) D. Braga and F. Grepioni, Intermolecular Interactions in Nonorganic Crystal Engineering, *Acc. Chem. Res.*, 2000, **33**, 601–608; (*b*) M. Shieh, Y.-H. Liu, Y.-H. Li and R. Y. Lin, Metal Carbonyl Cluster-Based Coordination Polymers: Diverse Syntheses, Versatile Network Structures, and Special Properties, *CrystEngComm*, 2019, **21**, 7341–7364.

45 (*a*) M. Shieh, C.-Y. Miu, Y.-Y. Chu and C.-N. Lin, Recent Progress in the Chemistry of Anionic Groups 6–8 Carbonyl Chalcogenide Clusters, *Coord. Chem. Rev.*, 2012, **256**, 637–694; (*b*) M. Shieh and C.-C. Yu, Ternary Copper-Incorporated Group 8 (Ru or Fe) Carbonyl Chalcogenide Complexes and Polymers: From Syntheses to Applications, *J. Organomet. Chem.*, 2017, **849–850**, 219–227.

46 (*a*) M. Shieh, C. Ho, W. Sheu, B. Chen, Y. Chu, C.-Y. Miu, H.-L. Liu and C.-C. Shen, Semiconducting Tellurium–Iron–Copper Carbonyl Polymers, *J. Am. Chem. Soc.*, 2008, **130**, 14114–14116; (*b*) M. Shieh, C.-C. Yu, C.-Y. Miu, C.-H. Kung, C.-Y. Huang, Y.-H. Liu, H.-L. Liu and C.-C. Shen, Semiconducting Coordination Polymers Based on the Predesigned Ternary Te–Fe–Cu Carbonyl Cluster and Conjugation-Interrupted Dipyridyl Linkers, *Chem.–Eur. J.*, 2017, **23**, 11261–11271.

47 (*a*) J.-C. P. Gabriel, K. Boubekeur, S. Uriel and P. Batail, Chemistry of Hexanuclear Rhenium Chalcohalide Clusters, *Chem. Rev.*, 2001, **101**, 2037–2066; (*b*) S. Jin and F. J. DiSalvo, 3D Coordination Network Structures Constructed from $[W_6S_8(CN)_6]^{6-}$ Anions, *Chem. Mater.*, 2002, **14**, 3448–3457.

48 C. A. Goddard, J. R. Long and R. H. Holm, Synthesis and Characterization of Four Consecutive Members of the Five-Member $[Fe_6S_8(PEt_3)_6]^{n+}$ $(n = 0 - 4)$ Cluster Electron Transfer Series, *Inorg. Chem.*, 1996, **35**, 4347–4354.

49 J. R. Long, L. S. McCarty and R. H. Holm, A Solid-State Route to Molecular Clusters: Access to the Solution Chemistry of $[Re_6Q_8]^{2+}$ (Q = S, Se) Core-Containing Clusters *via* Dimensional Reduction, *J. Am. Chem. Soc.*, 1996, **118**, 4603–4616.

50 (*a*) H. D. Selby, P. Orto, M. D. Carducci and Z. Zheng, Novel Concentration-Driven Structural Interconversion in Shape-Specific Solids Supported by the Octahedral $[Re_6(\mu_3\text{-}Se)_8]^{2+}$ Cluster Core, *Inorg. Chem.*, 2002, **41**, 6175–6177; (*b*) H. D. Selby, P. Orto and Z. Zheng, Supramolecular Arrays of the $[Re_6(\mu_3\text{-}Se)_8]^{2+}$ Core-Containing Clusters Mediated by Transition Metal Ions, *Polyhedron*, 2003, **22**, 2999–3008.

51 Y. M. Litvinova, Y. M. Gayfulin, K. A. Kovalenko, D. G. Samsonenko, J. van Leusen, I. V. Korolkov, V. P. Fedin and Y. V. Mironov, Multifunctional Metal–Organic Frameworks Based on Redox-Active Rhenium Octahedral Clusters, *Inorg. Chem.*, 2018, **57**, 2072–2084.

52 A. M. Champsaur, A. Velian, D. W. Paley, B. Choi, X. Roy, M. L. Steigerwald and C. Nuckolls, Building Diatomic and Triatomic Superatom Molecules, *Nano Lett.*, 2016, **16**, 5273–5277.

53 A. M. Champsaur, J. Yu, X. Roy, D. W. Paley, M. L. Steigerwald, C. Nuckolls and C. M. Bejger, Two-Dimensional Nanosheets from Redox-Active Superatoms, *ACS Cent. Sci.*, 2017, **3**, 1050–1055.

54 (*a*) M. B. Freeman, L. Wang, D. S. Jones and C. M. Bejger, A Cobalt Sulfide Cluster-Based Catholyte for Aqueous Flow Battery Applications, *J. Mater. Chem. A*, 2018, **6**, 21927–21932; (*b*) M. B. Freeman, O. D. Edokobi, J. H. Gillen, M. Kocherga, K. M. Dipple, D. S. Jones, D. W. Paley, L. Wang and C. M. Bejger, Stepwise Assembly of an Electroactive Framework from a Co_6S_8 Superatomic Metalloligand and Cuprous Iodide Building Units, *Chem.–Eur. J.*, 2020, DOI: 10.1002/chem.202001215.

55 (*a*) J. B. Howard and D. C. Rees, Structural Basis of Biological Nitrogen Fixation, *Chem. Rev.*, 1996, **96**, 2965–2982; (*b*) R. R. Eady, Structure-Function Relationships of Alternative Nitrogenases, *Chem. Rev.*, 1996, **96**, 3013–3030; (*c*) H. Dobbek, L. Gremer, R. Kiefersauer, R. Huber and O. Meyer, Catalysis at a Dinuclear [CuSMo(O)OH] Cluster in a CO Dehydrogenase Resolved at 1.1 Å Resolution, *Proc. Natl. Acad. Sci. U. S. A.*, 2002, **99**, 15971–15976; (*d*) R. Hille, S. Dingwall and J. Wilcoxen, The Aerobic CO Dehydrogenase from Oligotropha Carboxidovorans, *JBIC, J. Biol. Inorg. Chem.*, 2015, **20**, 243–251; (*e*) D. Ghosh, S. Sinhababu, B. D. Santarsiero and N. P. Mankad, A W/Cu Synthetic Model for the Mo/Cu Cofactor of Aerobic CODH Indicates That Biochemical CO Oxidation Requires a Frustrated Lewis Acid/Base Pair, *J. Am. Chem. Soc.*, 2020, DOI: 10.1021/jacs.0c03343.s001.

56 (*a*) H. Hou, Mo (W,V)–Cu (Ag)–S(Se) Cluster Compounds, *Coord. Chem. Rev.*, 1996, **153**, 25–56; (*b*) J. Lang, Structural Aspects of Copper(i) and Silver(i) Sulfide Clusters of Pentamethylcyclopentadienyl Trisulfido Tungsten(vi) and Molybdenum(vi), *Coord. Chem. Rev.*, 2003, **241**, 47–60; (*c*) C. Zhang, Y. Song and X. Wang, Correlations between Molecular Structures and Third-Order Non-Linear Optical Functions of Heterothiometallic Clusters: A Comparative Study, *Coord. Chem. Rev.*, 2007, **251**, 111–141.

57 (*a*) W.-H. Zhang, Y.-L. Song, Y. Zhang and J.-P. Lang, Binuclear Cluster-to-Cluster-Based Supramolecular Compounds: Design, Assembly, and Enhanced Third-Order Nonlinear Optical Performances of $\{[Et_4N]_2[MoOS_3Cu_2(\mu\text{-}CN)]_2 \cdot 2\text{aniline}\}_n$ and $\{[Et_4N]_4[MoOS_3Cu_3CN(\mu\text{-}CN)]_2(\mu\text{-}CN)_2\}_n$, *Cryst. Growth Des.*, 2008, **8**, 253–258; (*b*) J.-P. Lang, Q.-F. Xu, R.-X. Yuan and B. F. Abrahams, $\{[WS_4Cu_4(4,4'\text{-bpy})_4][WS_4Cu_4I_4(4,4'\text{-bpy})_2]\}_\infty$—an Unusual 3D Porous Coordination Polymer Formed from the Preformed Cluster $[Et_4N]_4[WS_4Cu_4I_6]$, *Angew. Chem., Int. Ed.*, 2004, **43**, 4741–4745; (*c*) W.-H. Zhang, Q. Liu and J.-P. Lang, Heterometallic Transition Metal Clusters and Cluster-Supported Coordination Polymers Derived from Tp- and Tp*-Based Mo(W) Sulfido Precursors, *Coord. Chem. Rev.*, 2015, **293–294**, 187–210; (*d*) W.-H. Zhang, Z.-G. Ren and J.-P. Lang, Rational Construction of Functional Molybdenum (Tungsten)–Copper–Sulfur Coordination Oligomers and Polymers from Preformed Cluster Precursors, *Chem. Soc. Rev.*, 2016, **45**, 4995–5019; (*e*) Q. Liu, W.-H. Zhang and J.-P. Lang, Versatile Thiomolybdate(Thiotungstate)–

Copper–Sulfide Clusters and Multidimensional Polymers Linked by Cyanides, *Coord. Chem. Rev.*, 2017, **350**, 248–274.

58 (*a*) W. H. Zhang, Y. L. Song, Z. G. Ren, H. X. Li, L. L. Li, Y. Zhang and J. P. Lang, Construction of $[(\eta^5\text{-}C_5Me_5)MoS_3Cu_3]$-Based Supramolecular Assemblies from the $[(\eta^5\text{-}C_5Me_5)MoS_3(CuNCS)_3]$-Cluster Anion and Multitopic Ligands with Different Symmetries, *Inorg. Chem.*, 2007, **46**, 6647–6660; (*b*) W. H. Zhang, Y. L. Song, Z. H. Wei, L. L. Li, Y. J. Huang, Y. Zhang and J. P. Lang, Assembly of $[(\eta^5\text{-}C_5Me_5)MoS_3Cu_3]$-Supported One-Dimensional Chains with Single, Double, Triple, and Quadruple Strands, *Inorg. Chem.*, 2008, **47**, 5332–5346.

59 J. Grote, F. Friedrich, K. Berthold, L. Hericks, B. Neumann, H.-G. Stammler and N. W. Mitzel, Dithiocarboxylic Acids: An Old Theme Revisited and Augmented by New Preparative, Spectroscopic and Structural Facts, *Chem.–Eur. J.*, 2018, **24**, 2626–2633.

60 N. E. Horwitz, E. V. Shevchenko, J. Park, E. Lee, J. Xie, B. Chen, Y. Zhong, A. S. Filatov and J. S. Anderson, Synthesis, Modular Composition, and Electrochemical Properties of Lamellar Iron Sulfides, *J. Mater. Chem. A*, 2020, DOI: 10.1039/d0ta00689k.

61 L. Sun, S. S. Park, D. Sheberla and M. Dincă, Measuring and Reporting Electrical Conductivity in Metal–Organic Frameworks: Cd_2(TTFTB) as a Case Study, *J. Am. Chem. Soc.*, 2016, **138**, 14772–14782.

62 (*a*) A. M. Evans, L. R. Parent, N. C. Flanders, R. P. Bisbey, E. Vitaku, M. S. Kirschner, R. D. Schaller, L. X. Chen, N. C. Gianneschi and W. R. Dichtel, Seeded Growth of Single-Crystal Two-Dimensional Covalent Organic Frameworks, *Science*, 2018, **361**, 52–57; (*b*) T. Ma, E. A. Kapustin, S. X. Yin, L. Liang, Z. Zhou, J. Niu, L.-H. Li, Y. Wang, J. Su, J. Li, X. Wang, W. D. Wang, W. Wang, J. Sun and O. M. Yaghi, Single-Crystal X-Ray Diffraction Structures of Covalent Organic Frameworks, *Science*, 2018, **361**, 48–52.

63 B. J. Smith and W. R. Dichtel, Mechanistic Studies of Two-Dimensional Covalent Organic Frameworks Rapidly Polymerized from Initially Homogenous Conditions, *J. Am. Chem. Soc.*, 2014, **136**, 8783–8789.

64 (*a*) G. C. Shearer, S. Chavan, S. Bordiga, S. Svelle, U. Olsbye and K. P. Lillerud, Defect Engineering: Tuning the Porosity and Composition of the Metal–Organic Framework UiO-66 *via* Modulated Synthesis, *Chem. Mater.*, 2016, **28**, 3749–3761; (*b*) L. Feng, K.-Y. Wang, J. Powell and H.-C. Zhou, Controllable Synthesis of Metal–Organic Frameworks and Their Hierarchical Assemblies, *Matter*, 2019, **1**, 801–824.

65 (*a*) D. L. Turner, T. P. Vaid, P. W. Stephens, K. H. Stone, A. G. DiPasquale and A. L. Rheingold, Semiconducting Lead–Sulfur–Organic Network Solids, *J. Am. Chem. Soc.*, 2008, **130**, 14–15; (*b*) D. L. Turner, K. H. Stone, P. W. Stephens and T. P. Vaid, Cadmium and Zinc Thiolate and Selenolate Metal–Organic Frameworks, *Dalton Trans.*, 2010, **39**, 5070–5073; (*c*) D. L. Turner, K. H. Stone, P. W. Stephens, A. Walsh, M. P. Singh and T. P. Vaid, Synthesis, Characterization, and Calculated Electronic Structure of the Crystalline Metal–Organic Polymers $[Hg(SC_6H_4S)(en)]_n$ and $[Pb(SC_6H_4S)(dien)]_n$, *Inorg. Chem.*, 2012, **51**, 370–376; (*d*) J. Park, A. C. Hinckley, Z. Huang, D. Feng, A. A. Yakovenko, M. Lee, S. Chen, X. Zou and Z. Bao, Synthetic Routes for a 2D Semiconductive Copper Hexahydroxybenzene Metal–Organic Framework, *J. Am. Chem. Soc.*, 2018, **140**, 14533–14537.

66 (*a*) J. Yu, J. Li, W. Zhang and H. Chang, Synthesis of High Quality Two-Dimensional Materials *via* Chemical Vapor Deposition, *Chem. Sci.*, 2015, **6**, 6705–6716; (*b*) Z. Cai, B. Liu, X. Zou and H.-M. Cheng, Chemical Vapor Deposition Growth and Applications of Two-Dimensional Materials and Their Heterostructures, *Chem. Rev.*, 2018, **118**, 6091–6133; (*c*) T. Zhang and L. Fu, Controllable Chemical Vapor Deposition Growth of Two-Dimensional Heterostructures, *Chem*, 2018, **4**, 671–689; (*d*) Y. Zhang, Y. Yao, M. G. Sendeku, L. Yin, X. Zhan, F. Wang, Z. Wang and J. He, Recent Progress in CVD Growth of 2D Transition Metal Dichalcogenides and Related Heterostructures, *Adv. Mater.*, 2019, **31**, 1901694.

67 (*a*) H. Maeda, R. Sakamoto and H. Nishihara, Coordination Programming of Two-Dimensional Metal Complex Frameworks, *Langmuir*, 2016, **32**, 2527–2538; (*b*) R. Dong, T. Zhang and X. Feng, Interface-Assisted Synthesis of 2D Materials: Trend and Challenges, *Chem. Rev.*, 2018, **118**, 6189–6325; (*c*) T. Pal, S. Doi, H. Maeda, K. Wada, C. M. Tan, N. Fukui, R. Sakamoto, S. Tsuneyuki, S. Sasaki and H. Nishihara, Interfacial Transmetallation Synthesis of a Platinadithiolene Nanosheet as a Potential 2D Topological Insulator, *Chem. Sci.*, 2019, **10**, 5218–5225.

68 (*a*) R. Dong, M. Pfeffermann, H. Liang, Z. Zheng, X. Zhu, J. Zhang and X. Feng, Large-Area, Free-Standing, Two-Dimensional Supramolecular Polymer Single-Layer Sheets for Highly Efficient Electrocatalytic Hydrogen Evolution, *Angew. Chem., Int. Ed.*, 2015, **54**, 12058–12063; (*b*) Y. Zhong, B. Cheng, C. Park, A. Ray, S. Brown, F. Mujid, J.-U. Lee, H. Zhou, J. Suh, K.-H. Lee, A. J. Mannix, K. Kang, S. J. Sibener, D. A. Muller and J. Park, Wafer-Scale Synthesis of Monolayer Two-Dimensional Porphyrin Polymers for Hybrid Superlattices, *Science*, 2019, **366**, 1379–1384.

69 (*a*) R. Llusar and C. Vicent, Trinuclear Molybdenum Cluster Sulfides Coordinated to Dithiolene Ligands and Their Use in the Development of Molecular Conductors, *Coord. Chem. Rev.*, 2010, **254**, 1534–1548; (*b*) E. Dornsiepen, F. Pieck, R. Tonner and S. Dehnen, $[\{(PhSn)_3SnS_6\}\{(MCp)_3S_4\}]$ (M = W, Mo): Minimal Molecular Models of the Covalent Attachment of Metal Chalcogenide Clusters on Doped Transition Metal Dichalcogenide Layers, *J. Am. Chem. Soc.*, 2019, **141**, 16494–16500.

70 (*a*) M. J. Allen, V. C. Tung and R. B. Kaner, Honeycomb Carbon: A Review of Graphene, *Chem. Rev.*, 2010, **110**, 132–145; (*b*) K. S. Novoselov, V. I. Fal'ko, L. Colombo, P. R. Gellert, M. G. Schwab and K. Kim, A Roadmap for Graphene, *Nature*, 2012, **490**, 192–200.

71 S. Manzeli, D. Ovchinnikov, D. Pasquier, O. V. Yazyev and A. Kis, 2D Transition Metal Dichalcogenides, *Nat. Rev. Mater.*, 2017, **2**, 17033.

72 (*a*) D. Sheberla, L. Sun, M. a. Blood-forsythe, S. Er, C. R. Wade, C. K. Brozek, A. Aspuru-guzik, M. Dincă, R. Casey, C. K. Brozek, A. Aspuru-guzik, M. Dinc and S. Experimental, A Semiconducting Metal–Organic Graphene Analogue Supporting Information, *J. Am. Chem. Soc.*, 2014, **3**, 1–13; (*b*) B. Hoppe, K. D. J. Hindricks, D. P. Warwas, H. A. Schulze, A. Mohmeyer, T. J. Pinkvos, S. Zailskas, M. R. Krey, C. Belke, S. König, M. Fröba, R. J. Haug and P. Behrens, Graphene-like Metal–Organic Frameworks: Morphology Control, Optimization of Thin Film Electrical Conductivity and Fast Sensing Applications, *CrystEngComm*, 2018, **20**, 6458–6471.

73 K. F. Mak and J. Shan, Photonics and Optoelectronics of 2D Semiconductor Transition Metal Dichalcogenides, *Nat. Photonics*, 2016, **10**, 216–226.

74 (*a*) M. Eddaoudi, D. B. Moler, H. Li, B. Chen, T. M. Reineke, M. O'Keeffe and O. M. Yaghi, Modular Chemistry: Secondary Building Units as a Basis for the Design of Highly Porous and Robust Metal–Organic Carboxylate Frameworks, *Acc. Chem. Res.*, 2001, **34**, 319–330; (*b*) M. J. Kalmutzki, N. Hanikel and O. M. Yaghi, Secondary Building Units as the Turning Point in the Development of the Reticular Chemistry of MOFs, *Sci. Adv.*, 2018, **4**, eaat9180.

75 (*a*) D. Feng, K. Wang, Z. Wei, Y.-P. Chen, C. M. Simon, R. K. Arvapally, R. L. Martin, M. Bosch, T.-F. Liu, S. Fordham, D. Yuan, M. A. Omary, M. Haranczyk, B. Smit and H.-C. Zhou, Kinetically Tuned Dimensional Augmentation as a Versatile Synthetic Route towards Robust Metal–Organic Frameworks, *Nat. Commun.*, 2014, **5**, 5723; (*b*) M. Bosch, S. Yuan, W. Rutledge and H.-C. Zhou, Stepwise Synthesis of Metal–Organic Frameworks, *Acc. Chem. Res.*, 2017, **50**, 857–865.

76 (*a*) C. Serre, F. Millange, S. Surblé and G. Férey, A Route to the Synthesis of Trivalent Transition-Metal Porous Carboxylates with Trimeric Secondary Building Units, *Angew. Chem., Int. Ed.*, 2004, **43**, 6285–6289; (*b*) V. Guillerm, S. Gross, C. Serre, T. Devic, M. Bauer and G. Férey, A Zirconium Methacrylate Oxocluster as Precursor for the Low-Temperature Synthesis of Porous Zirconium(iv) Dicarboxylates, *Chem. Commun.*, 2010, **46**, 767–769; (*c*) K. Wang, D. Feng, T.-F. Liu, J. Su, S. Yuan, Y.-P. Chen, M. Bosch, X. Zou and H.-C. Zhou, A Series of Highly Stable Mesoporous Metalloporphyrin Fe–MOFs, *J. Am. Chem. Soc.*, 2014, **136**, 13983–13986.

77 (*a*) M. Duchardt, S. Neuberger, U. Ruschewitz, T. Krauskopf, W. G. Zeier, J. Schmedt auf der Günne, S. Adams, B. Roling and S. Dehnen, Superion Conductor $Na_{11.1}Sn_{2.1}P_{0.9}Se_{12}$: Lowering the Activation Barrier of Na^+ Conduction in Quaternary 1–4–5–6 Electrolytes, *Chem. Mater.*, 2018, **30**, 4134–4139; (*b*) Y. Zheng, S. Zheng, H. Xue and H. Pang, Metal–Organic Frameworks for Lithium–Sulfur Batteries, *J. Mater. Chem. A*, 2019, **7**, 3469–3491.

78 K.-K. Yee, N. Reimer, J. Liu, S.-Y. Cheng, S.-M. Yiu, J. Weber, N. Stock and Z. Xu, Effective Mercury Sorption by Thiol-Laced Metal–Organic Frameworks: In Strong Acid and the Vapor Phase, *J. Am. Chem. Soc.*, 2013, **135**, 7795–7798.

79 L. Ding, X. Luo, P. Shao, J. Yang and D. Sun, Thiol-Functionalized Zr-Based Metal–Organic Framework for Capture of Hg(ii) through a Proton Exchange Reaction, *ACS Sustainable Chem. Eng.*, 2018, **6**, 8494–8502.

80 (*a*) S. S. Park, Y. Tulchinsky and M. Dincă, Single-Ion Li^+, Na^+, and Mg^{2+} Solid Electrolytes Supported by a Mesoporous Anionic Cu–Azolate Metal–Organic Framework, *J. Am. Chem. Soc.*, 2017, **139**, 13260–13263; (*b*) E. M. Miner, S. S. Park and M. Dincă, High Li^+ and Mg^{2+} Conductivity in a Cu–Azolate Metal–Organic Framework, *J. Am. Chem. Soc.*, 2019, **141**, 4422–4427; (*c*) B. M. Wiers, M.-L. Foo, N. P. Balsara and J. R. Long, A Solid Lithium Electrolyte *via* Addition of Lithium Isopropoxide to a Metal–Organic Framework with Open Metal Sites, *J. Am. Chem. Soc.*, 2011, **133**, 14522–14525.

81 X.-F. Liu, X.-Q. Guo, R. Wang, Q.-C. Liu, Z.-J. Li, S.-Q. Zang and T. C. W. Mak, Manganese Cluster-Based MOF as Efficient Polysulfide-Trapping Platform for High-Performance Lithium–Sulfur Batteries, *J. Mater. Chem. A*, 2019, **7**, 2838–2844.

82 Z. Zheng, Chemical Transformations Supported by the $[Re_6(\mu_3\text{-}Se)_8]^{2+}$ Cluster Core, *Dalton Trans.*, 2012, **41**, 5121–5131.

83 Z. Zheng and X. Tu, Crystal Engineering Supported by the $[Re_6(\mu_3\text{-}Se)_8]^{2+}$ Core-Containing Clusters, *CrystEngComm*, 2009, **11**, 707–719.

84 (*a*) F. Li, R. L. Meyer, S. H. Carpenter, L. E. VanGelder, A. W. Nichols, C. W. Machan, M. L. Neidig and E. M. Matson, Nitric Oxide Activation Facilitated by Cooperative Multimetallic Electron Transfer within an Iron-Functionalized Polyoxovanadate–Alkoxide Cluster, *Chem. Sci.*, 2018, **9**, 6379–6389; (*b*) B. E. Petel, W. W. Brennessel and E. M. Matson, Oxygen-Atom Vacancy Formation at Polyoxovanadate Clusters: Homogeneous Models for Reducible Metal Oxides, *J. Am. Chem. Soc.*, 2018, **140**, 8424–8428; (*c*) B. E. Petel, R. L. Meyer, W. W. Brennessel and E. M. Matson, Oxygen Atom Transfer with Organofunctionalized Polyoxovanadium Clusters: O–Atom Vacancy Formation with Tertiary Phosphanes and Deoxygenation of Styrene Oxide, *Chem. Sci.*, 2019, **10**, 8035–8045; (*d*) L. Chen, K. A. San, M. J. Turo, M. Gembicky, S. Fereidouni, M. Kalaj and A. M. Schimpf, Tunable Metal Oxide Frameworks *via* Coordination Assembly of Preyssler-Type Molecular Clusters, *J. Am. Chem. Soc.*, 2019, **141**, 20261–20268; (*e*) L. Chen, M. J. Turo, M. Gembicky, R. A. Reinicke and A. M. Schimpf, Cation-Controlled Assembly of Polyoxotungstate-Based Coordination Networks, *Angew. Chem., Int. Ed.*, 2020, DOI: 10.1002/anie.202005627.

85 (*a*) N. Van Velthoven, S. Waitschat, S. M. Chavan, P. Liu, S. Smolders, J. Vercammen, B. Bueken, S. Bals, K. P. Lillerud, N. Stock and D. E. De Vos, Single-Site

Metal–Organic Framework Catalysts for the Oxidative Coupling of Arenes *via* C–H/C–H Activation, *Chem. Sci.*, 2019, **10**, 3616–3622; (*b*) X. Feng, Y. Song, J. S. Chen, Z. Li, E. Y. Chen, M. Kaufmann, C. Wang and W. Lin, Cobalt-Bridged Secondary Building Units in a Titanium Metal–Organic Framework Catalyze Cascade Reduction of N-Heteroarenes, *Chem. Sci.*, 2019, **10**, 2193–2198; (*c*) Y. Song, Z. Li, P. Ji, M. Kaufmann, X. Feng, J. S. Chen, C. Wang and W. Lin, Metal–Organic Framework Nodes Support Single-Site Nickel(ii) Hydride Catalysts for the Hydrogenolysis of Aryl Ethers, *ACS Catal.*, 2019, **9**, 1578–1583; (*d*) X. Feng, P. Ji, Z. Li, T. Drake, P. Oliveres, E. Y. Chen, Y. Song, C. Wang and W. Lin, Aluminum Hydroxide Secondary Building Units in a Metal–Organic Framework Support Earth-Abundant Metal Catalysts for Broad-Scope Organic Transformations, *ACS Catal.*, 2019, **9**, 3327–3337.

86 J. A. Kephart, B. S. Mitchell, A. Chirila, K. J. Anderton, D. Rogers, W. Kaminsky and A. Velian, Atomically Defined Nano-Propeller Fe_3 $Co_6Se_8(Ph_2PNTol)_6$: Functional Model for the Electronic Metal-Support Interaction Effect, and High Catalytic Activity for Carbodiimide Formation, *J. Am. Chem. Soc.*, 2019, **141**, 19605–19610.

87 (*a*) G. Lan, Y. Quan, M. Wang, G. T. Nash, E. You, Y. Song, S. S. Veroneau, X. Jiang and W. Lin, Metal–Organic Layers as Multifunctional Two-Dimensional Nanomaterials for Enhanced Photoredox Catalysis, *J. Am. Chem. Soc.*, 2019, **141**, 15767–15772; (*b*) L. Zeng, Z. Wang, Y. Wang, J. Wang, Y. Guo, H. Hu, X. He, C. Wang and W. Lin, Photoactivation of Cu Centers in Metal–Organic Frameworks for Selective CO_2 Conversion to Ethanol, *J. Am. Chem. Soc.*, 2020, **142**, 75–79.

88 (*a*) K. Mizushima, P. C. Jones, P. J. Wiseman and J. B. Goodenough, Li_xCoO_2 ($0 < x < -1$): A New Cathode Material for Batteries of High Energy Density, *Mater. Res. Bull.*, 1980, **15**, 783–789; (*b*) A. K. Padhi, Effect of Structure on the Fe^{3+}/Fe^{2+} Redox Couple in Iron Phosphates, *J. Electrochem. Soc.*, 1997, **144**, 1609–1613.

89 (*a*) J. Calbo, M. J. Golomb and A. Walsh, Redox-Active Metal–Organic Frameworks for Energy Conversion and Storage, *J. Mater. Chem. A*, 2019, **7**, 16571–16597; (*b*) J. Liu, X. Song, T. Zhang, S. Liu, H. Wen and L. Chen, 2D Conductive Metal–Organic Frameworks: An Emerging Platform for Electrochemical Energy Storage, *Angew. Chem., Int. Ed.*, 2020, DOI: 10.1002/anie.202006102.

90 M. E. Ziebel, C. A. Gaggioli, A. B. Turkiewicz, W. Ryu, L. Gagliardi and J. R. Long, Effects of Covalency on Anionic Redox Chemistry in Semiquinoid-Based Metal–Organic Frameworks, *J. Am. Chem. Soc.*, 2020, **142**, 2653–2664.

91 T. Li, Y.-H. Liu, B. Chitara and J. E. Goldberger, Li Intercalation into 1D TiS_2(en) Chains, *J. Am. Chem. Soc.*, 2014, **136**, 2986–2989.

92 (*a*) D. Sheberla, J. C. Bachman, J. S. Elias, C.-J. Sun, Y. Shao-Horn and M. Dincă, Conductive MOF Electrodes for Stable Supercapacitors with High Areal Capacitance, *Nat. Mater.*, 2017, **16**, 220–224; (*b*) S. Bi, H. Banda, M. Chen, L. Niu, M. Chen, T. Wu, J. Wang, R. Wang, J. Feng, T. Chen, M. Dincă, A. A. Kornyshev and G. Feng, Molecular Understanding of Charge Storage and Charging Dynamics in Supercapacitors with MOF Electrodes and Ionic Liquid Electrolytes, *Nat. Mater.*, 2020, **19**, 552–558.

93 D. Feng, T. Lei, M. R. Lukatskaya, J. Park, Z. Huang, M. Lee, L. Shaw, S. Chen, A. A. Yakovenko, A. Kulkarni, J. Xiao, K. Fredrickson, J. B. Tok, X. Zou, Y. Cui and Z. Bao, Robust and Conductive Two-Dimensional Metal–organic Frameworks with Exceptionally High Volumetric and Areal Capacitance, *Nat. Energy*, 2018, **3**, 30–36.

94 C. Choi, D. S. Ashby, D. M. Butts, R. H. DeBlock, Q. Wei, J. Lau and B. Dunn, Achieving High Energy Density and High Power Density with Pseudocapacitive Materials, *Nat. Rev. Mater.*, 2020, **5**, 5–19.

95 Q. Mahmood, M. G. Kim, S. Yun, S.-M. Bak, X.-Q. Yang, H. S. Shin, W. S. Kim, P. V. Braun and H. S. Park, Unveiling Surface Redox Charge Storage of Interacting Two-Dimensional Heteronanosheets in Hierarchical Architectures, *Nano Lett.*, 2015, **15**, 2269–2277.

96 (*a*) S. A. Wolf, Spintronics: A Spin-Based Electronics Vision for the Future, *Science*, 2001, **294**, 1488–1495; (*b*) D. D. Awschalom and M. E. Flatté, Challenges for Semiconductor Spintronics, *Nat. Phys.*, 2007, **3**, 153–159; (*c*) J. Linder and J. W. A. Robinson, Superconducting Spintronics, *Nat. Phys.*, 2015, **11**, 307–315; (*d*) E. Coronado, Molecular Magnetism: From Chemical Design to Spin Control in Molecules, Materials and Devices, *Nat. Rev. Mater.*, 2020, **5**, 87–104.

97 (*a*) J. E. Moore, The Birth of Topological Insulators, *Nature*, 2010, **464**, 194–198; (*b*) D. Kong and Y. Cui, Opportunities in Chemistry and Materials Science for Topological Insulators and Their Nanostructures, *Nat. Chem.*, 2011, **3**, 845–849; (*c*) B. Bradlyn, L. Elcoro, J. Cano, M. G. Vergniory, Z. Wang, C. Felser, M. I. Aroyo and B. A. Bernevig, Topological Quantum Chemistry, *Nature*, 2017, **547**, 298–305; (*d*) P. Liu, J. R. Williams and J. J. Cha, Topological Nanomaterials, *Nat. Rev. Mater.*, 2019, **4**, 479–496; (*e*) Y. Tokura, K. Yasuda and A. Tsukazaki, Magnetic Topological Insulators, *Nat. Rev. Phys.*, 2019, **1**, 126–143.

98 (*a*) X. G. Wen, Four Revolutions in Physics and the Second Quantum Revolution-A Unification of Force and Matter by Quantum Information, *Int. J. Mod. Phys. B*, 2018, **32**, 1–24; (*b*) M. Atzori and R. Sessoli, The Second Quantum Revolution: Role and Challenges of Molecular Chemistry, *J. Am. Chem. Soc.*, 2019, **141**, 11339–11352.

99 (*a*) S. Manipatruni, D. E. Nikonov, C.-C. Lin, T. A. Gosavi, H. Liu, B. Prasad, Y.-L. Huang, E. Bonturim, R. Ramesh and I. A. Young, Scalable Energy-Efficient Magnetoelectric Spin–Orbit Logic, *Nature*, 2019, **565**, 35–42; (*b*) X. Lin, W. Yang, K. L. Wang and W. Zhao, Two-Dimensional Spintronics for Low-Power Electronics, *Nat. Electron.*, 2019, **2**, 274–283.

100 (*a*) Z. F. Wang, N. Su and F. Liu, Prediction of a Two-Dimensional Organic Topological Insulator, *Nano Lett.*, 2013, **13**, 2842–2845; (*b*) C. Chakravarty, B. Mandal and

P. Sarkar, Bis(Dithioline)-Based Metal–Organic Frameworks with Superior Electronic and Magnetic Properties: Spin Frustration to Spintronics and Gas Sensing, *J. Phys. Chem. C*, 2016, **120**, 28307–28319; (*c*) L.-C. Zhang, L. Zhang, G. Qin, Q.-R. Zheng, M. Hu, Q.-B. Yan and G. Su, Two-Dimensional Magnetic Metal–Organic Frameworks with the Shastry-Sutherland Lattice, *Chem. Sci.*, 2019, **10**, 10381–10387; (*d*) L. Yang, X. He and M. Dincă, Triphenylene-Bridged Trinuclear Complexes of Cu: Models for Spin Interactions in Two-Dimensional Electrically Conductive Metal–Organic Frameworks, *J. Am. Chem. Soc.*, 2019, **141**, 10475–10480; (*e*) L. Liu, J. A. DeGayner, L. Sun, D. Z. Zee and T. D. Harris, Reversible Redox Switching of Magnetic Order and Electrical Conductivity in a 2D Manganese Benzoquinoid Framework, *Chem. Sci.*, 2019, **10**, 4652–4661; (*f*) C. Yang, R. Dong, M. Wang, P. S. Petkov, Z. Zhang, M. Wang, P. Han, M. Ballabio, S. A. Bräuninger, Z. Liao, J. Zhang, F. Schwotzer, E. Zschech, H.-H. Klauss, E. Cánovas, S. Kaskel, M. Bonn, S. Zhou, T. Heine and X. Feng, A Semiconducting Layered Metal–Organic Framework Magnet, *Nat. Commun.*, 2019, **10**, 3260.

101 (*a*) Y. Ma, L. Kou, X. Li, Y. Dai, S. C. Smith and T. Heine, Quantum Spin Hall Effect and Topological Phase Transition in Two-Dimensional Square Transition-Metal Dichalcogenides, *Phys. Rev. B: Condens. Matter Mater. Phys.*, 2015, **92**, 085427; (*b*) P. Chen, W. W. Pai, Y.-H. Chan, W.-L. Sun, C.-Z. Xu, D.-S. Lin, M. Y. Chou, A.-V. Fedorov and T.-C. Chiang, Large Quantum-Spin-Hall Gap in Single-Layer 1T′ WSe_2, *Nat. Commun.*, 2018, **9**, 2003; (*c*) M. M. Ugeda, A. Pulkin, S. Tang, H. Ryu, Q. Wu, Y. Zhang, D. Wong, Z. Pedramrazi, A. Martín-Recio, Y. Chen, F. Wang, Z.-X. Shen, S.-K. Mo, O. V. Yazyev and M. F. Crommie, Observation of Topologically Protected States at Crystalline Phase Boundaries in Single-Layer WSe_2, *Nat. Commun.*, 2018, **9**, 3401.